Highlights of Joint Research

Synchrotron Radiation Laboratory

The Synchrotron Radiation Laboratory (SRL) was established in 1975 as a research division dedicating to solid state physics using synchrotron radiation. In 1989, SRL started to hold the Tsukuba branch, a branch laboratory in the Photon Factory (PF), High Energy Accelerator Research Organization (KEK). SRL maintains a Revolver undulator, two beamlines and three experimental stations; BL-18A for angle-resolved photoemission spectroscopy with SCIENTA SES100 energy analyser and undulator beamline BL-19A and BL-19B, for spin- and angle-resolved photoelectron spectroscopy (SARPES) and soft X-ray emission spectroscopy experiments, respectively. They are fully opened to outside users for experiments using high brilliant synchrotron radiation. The operation time of these beamlines are about 4000 hours and the number of users is more than 100 a year. In 2009, the new spin detector adopting VLEED has been utilized to investigate those, such as topological insulators and quantum films with Rashba splitting surface states, which have been the exciting topics in surface and solid state physics and strongly demand high resolution spin-resolved photoemission spectra. The staff members of SRL have been not only serving users with technical supports and advices, but also carrying out their own research works on advanced solid state spectroscopy.

SRL also participates to the Materials Research Division of the Synchrotron Radiation Research Organization of the University of Tokyo (SRRO) and plays essential roles in promoting scientific activities at the new soft X-ray undulator beamline, BL07-LSU in SPring-8. The beamline consists of the polarization controlled 25-m long soft X-ray undulator and varied line spacing plain grating monochromator which covers the energy range between 250 eV and 2 keV. In the end section of the beamline, it is equipped with experimental apparatuses using high brilliance synchrotron radiation in soft X-ray region. After finishing the construction of the new beamline in 2009, SRL established the Harima branch laboratory in SPring-8 and since then, the staff members of SRL dedicated to apply the high brilliance soft X-ray for the advanced solid state spectroscopy.

In 2010, we have confirmed that the main apparatuses at the beamline BL07-LSU, i.e. three-dimensional (3D) nano-ESCA, soft X-ray emission spectroscopy (XES) and time-resolved photoemission experimental stations, achieved high quality of performance as they initially expected: 3D nano-ESCA showed the spatial resolution below 70 nm,

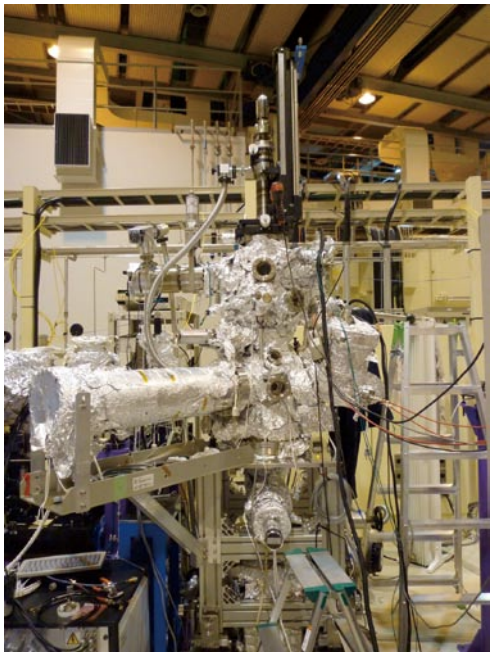

Fig. 1. Time- and momentum-resolved soft X-ray spectrometer installed at BL07LSU

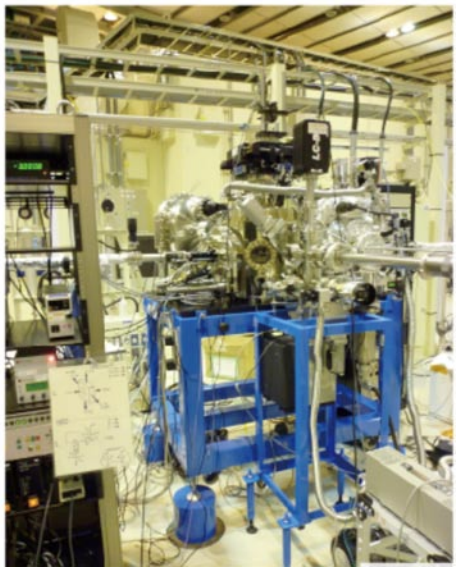

Fig.2. 3D nano-ESCA; ARPES spectrometer for 3D analyses of electronic structures of nano-fablicated materials

Fig.3. High resolution soft X-ray emission spectrometer at BL07LSU

XES spectra with energy resolution lager than 10,000 was obtained and time- and momentum-resolved photoemission spectra were measured synchronized with femto-second laser pulses. The four vertical figure-8 undulator segments were inserted into the 25-m long straight section of SPring-8 in summer of 2010. Together with four horizontal figure-8 undulator segments, they will be able to produce the polarization controlled undulator light in near future.

A few members of SRL have been dedicating to research works on the accelerator physics and developing various new accelerator related technology in collaboration with other SR facilities. They study future ERL (energy recovery linac) light source and developed ERL components in collaboration with KEK, AIST and JAEA, main works of which are carried out both in Kashiwa campus and at KEK in Tsukuba.

Supercomputer Center

The Supercomputer Center (SCC) is a part of the Materials Design and Characterization Laboratory (MDCL) of ISSP. Its mission is to serve the whole community of computational condensed-matter physics of Japan with high performance computing environment. In particular, the SCC selectively promotes and supports large-scale computations. For this purpose, the SCC invites proposals for supercomputer-aided research projects and hosts the Steering Committee, as mentioned below, that evaluates the proposals.

The ISSP supercomputer system consists of two subsystems: System A, which is intended for a parallel computation with relatively smaller number of nodes connected tightly, and System B, which is intended for more nodes with relatively loose connections. Until March 2009, System A was Hitachi SR11000/48 that consists of 48 high performance nodes whereas System B was SGI Altix 3700/1280.

In the school year 2010, the SCC made big steps forward. The SCC replaced the two supercomputer subsystems. The new system B is SGI Altix ICE 8400EX, which consists of 30 racks or 15360 cores whereas the new system A is NEC SX-9, which consists of 4 nodes or 64 cpus. The SCC started operating these machines in July, 2010, which provides the computational condensed-matter physics community with approximately 200 TFlops of computational power, more than 15 times greater computational resources than the old systems.

The hardware administration is not the only function of the SCC. The ISSP started hosting Computational Materials Science Initiative (CMSI), a new activity of promoting materials science study with next-generation parallel supercomputing. This activity is financially supported by the MEXT HPCI strategic program, and in CMSI, a number of major Japanese research institutes in various branches of materials science are involved. The SCC supports the activities of CMSI as its major mission.

All staff members of university faculties or public research institutes in Japan are invited to propose research projects (called User Program). The proposals are evaluated by the Steering Committee of SCC. Pre-reviewing is done by the Supercomputer Project Advisory Committee. In school year 2009 totally 181 projects were approved. The total points applied and approved are listed on Table. 1 below.

The research projects are roughly classified into the following three (the number of projects approved):

First-Principles Calculation of Materials Properties (80)
Strongly Correlated Quantum Systems (60)
Cooperative Phenomena in Complex, Macroscopic Systems (53)

All the three involve both methodology of computation and its applications. The results of the projects are reported in 'Activity Report 2010' of the SCC. Everyyear 3-4 projects are selected for “invited papers” and published at the beginning of the Activity Report. In the Activity Report 2010, the following three invited papers are included:

“Numerical-Diagonalization Study of the Heisenberg Antiferromagnet on the Kagome Lattice”
Hiroki NAKANO and Toru SAKAI
“Extended Loop Algorithm for Pyrochlore Heisenberg Spin Models with Spin-Ice Type Degeneracy: Application to Spin-Glass Transition in Antiferromagnets Coupled to Local Lattice Distortions”
Hiroshi SHINAOKA
“Real-Time TDDFT Simulation for Light-Induced Electron-Phonon Dynamics in Dielectrics”
Kazuhiro YABANA and Yasushi SHINOHARA

Class	Max/Min Points	Application	Number of Projects	Total Points			
				Applied		Approved	
				System A	System B	System A	System B
A	<100K	any time	0	0K	0K	0K	0K
B	<2M	twice a year	42	31K	48K	22K	35K
C	<20M	twice a year	142	1169K	1372K	887K	926K
D		any time	7	4K	92K	3K	76K
S	>20M	twice a year	1	0K	40K	0K	40K
Total			192	1204K	1552K	912K	1077K

Table 1. Research projects approved in 2010
The maximum points allotted to the project of each class are the sum of the points for the two systems; 1 point of System-A corresponds to charge for 1.11(→1.63) hours × node, while the corresponding figure is 0.52hours × 128CPU for System-B.

Neutron Science Laboratory

The Neutron Science Laboratory (NSL) has been playing a central role in neutron scattering activities in Japan since 1961 by performing its own research programs as well as providing a strong General User Program for the university-owned various neutron scattering spectrometers installed at the JRR-3 (20MW) operated by Japan Atomic Energy Agency (JAEA) in Tokai. In 2003, the Neutron Scattering Laboratory was reorganized as the Neutron Science Laboratory to further promote the neutron science with use of the instruments in JRR-3. Under the General User Program supported by NSL, 14 university-group-owned spectrometers in the JRR-3 reactor are available for a wide scope of researches on material science, and proposals close to 300 are submitted each year, and the number of visiting users under this program reaches over 6000 person-day/year. In 2009, NSL and Neutron Science Laboratory (KENS),

Fig. 1 The reactor hall of JRR-3. The eight neutron scattering instruments are attached to the horizontal beam tubes in the reactor experimental hall. Two thermal and three cold guides are extracted from the reactor core towards the guide hall located to the left.

High Energy Accelerator Research Organization (KEK) built a chopper spectrometer, High Resolution Chopper Spectrometer, HRC, at the beam line BL12 of MLF/J-PARC (Materials and Life Science Experimental Facility, J-PARC). HRC covers a wide energy and Q-range ($10\mu eV < \hbar\omega < 2eV$ and $0.02Å^{-1} < Q < 50Å^{-1}$), and therefore becomes complementary to the existing inelastic spectrometers at JRR-3. HRC started commissioning and trial user experiments through the S-type/IRT-project proposal in FY2010, and is expected to accept general users through the J-PARC proposal system in FY2011.

Triple axis spectrometers, HRC, and a high resolution powder diffractometer are utilized for a conventional solid state physics and a variety of research fields on hard-condensed matter, while in the field of soft-condensed matter science, researches are mostly carried out by using the small angle neutron scattering (SANS-U) and/or neutron spin echo (iNSE) instruments. The upgraded time-of-flight (TOF) inelastic scattering spectrometer is also available through the ISSP-NSL user program.

Major research topics on the hard-condensed matter science cover stripe order in high-T_c superconductors, and closely related 2 dimensional systems, charge and orbital ordering in CMR manganites, quadrupolar ordering in rare-earth based intermetallic compounds, spin dynamics of low dimensional dimer systems, etc. On the other hand, the research topics on the soft-condensed matter science cover structural characterization of polymer gels, polymer blends, micelles, amphiphilic polymers, block copolymers, proteins,

Fig. 2 Completion Ceremony of High Resolution Chopper Spectrometer (HRC) at the beam line BL12 of MLF/J-PARC (March 26, 2010).

dynamics of brush-polymers on surface, slow dynamics of surfactants, pressure dependence of dynamics of amphiphilic membranes, and so on. In addition, there are a variety of activities on fundamental physics, neutron beam optics, developments of neutron scattering techniques.

The NSL also operates the U.S.-Japan Cooperative Program on neutron scattering, providing further research opportunities to material scientists who utilize the neutron scattering technique for their research interests. In 2010, relocation of the U.S.-Japan triple-axis spectrometer, CTAX-2, was completed, and now the spectrometer is in the commissioning phase.

The activity report on Neutron Scattering Research in JFY2010 is given in NSL-ISSP Activity Report vol. 17 (2010), which can be downloaded from the following URL, http://quasi.issp.u-tokyo.ac.jp/actrep/actrep-17/index-rep_vol17.html

The list of publication is also given at, http://quasi.issp.u-tokyo.ac.jp/actrep/actrep-17/index-pub_vol17.html.

International MegaGauss Science Laboratory

The aim of this laboratory is to study the physical properties of solid-state materials (such as semiconductors, magnetic materials, metals, insulators, superconducting materials) under ultra-high magnetic field conditions. Such a high magnetic field is also used for controlling the new material phase and functions. Our pulse magnets, at moment, can generate up to 85 Tesla (T) by non-destructive manner, and from 100 up to 730 T (the world strongest as an in-door record) by destructive (the single turn coil and the electromagnetic flux compression) methods.

They are opened for scientists both from Japan and from overseas, especially from Asian countries, and many fruitful results are expected to come out not only from collaborative research but also from our in-house activities. One of our ultimate goals is to provide the scientific users as our joint research with magnets capable of a 100 T, milli-second pulses in a non-destructive mode, and to offer versatile physical precision measurements. The available measuring techniques now involve magneto-optical measurements, cyclotron resonance, spin resonance, magnetization and transport measurements.

Our interests cover the study on quantum phase transitions (QPT) induced by high magnetic fields. Field-induced QPT has been explored in various materials such as quantum spin systems, strongly correlated electron systems and other magnetic materials. Non-destructive strong pulse magnets are expected to provide us with reliable and precise solid state physics measurements. The number of collaborative groups for the research is over 50 in the year of 2010.

A 210 MJ flywheel generator which is the world largest DC power supply has been installed in the newly built DC flywheel generator station at our institute. The generator, once disassembled from the one used for toroidal magnetic field coil in JFT-2M (JAERI Fusion Torus-2M) tokamak nuclear fusion testing device, is now renewed as a power supply for the pulse magnets. The construction of the magnet service station has also been accomplished. The magnet

technologies are intensively devoted to the quasi-steady long pulse magnet (an order of 1-10 sec) energized by the giant DC power supply, and also used for the outer-magnet coil to realize a 100 T nondestructive magnet.

Developments of our destructive magnets are currently in progress. The ultra-high magnetic fields are obtained in a microsecond time scale. The electromagnetic flux compression (EMFC) system is equipped with a 5 MJ condenser bank and its seed coils with a 1.5 MJ condenser bank. The protector chamber and iron block protectors were refined against stronger explosion than before to be endurable for explosion by a full injection of 5 MJ. By devising copper lined primary coil, we could improve energy transfer efficiency from the primary coil to the liner kinetic energy compressing the magnetic flux. The seed field coils providing the initial magnetic flux are also newly designed and the maximum magnetic field was increased from 3.2 T to over 4.4 T at the position of the primary coil. These efforts led us to obtain the maximum magnetic field of 730 T by a 4 MJ injection of the EMFC recognized as a renewal of the world record as an indoor experiment. We have started a new project of the EMFC aiming at achieving1000 T and it's application to the materials science, financed by the ministry of education, culture, sports, science and technology in the 2010 and 2011 fiscal year.

As an easy access to the megagauss science and technology, we have the single-turn coil (STC) system capable of generating the fields of up to 200 T by a fast-capacitor of 200 kJ. We have two STC systems, one is a horizontal type (H-type) and the other is a vertical type (V-type). Various kinds of laser spectroscopy experiments such as the cyclotron resonance and the Faraday rotation using the H-type STC are available. On the other hand, for very low temperature experiment, a combination of the V-type STC and a liquid helium bath cryostat is very useful; the precise magnetization measurements at 2.5 K can be performed up to 120 T.

Fig. 1. The building for the flywheel generator (left hand side) and a long pulse magnet station (right hand side). The flywheel giant DC generator is 350 ton in weight and 5 m high (bottom). The generator, capable of a 51 mega watt out put power with a 210 mega joule energy storage, is planned to energize the long pulse magnet generating 100 Tesla without destruction.

Antiferroquadrupolar Ordering in a Pr-Based Superconductor $PrIr_2Zn_{20}$

T. Onimaru, T. Sakakibara, and M. Kubota

Orbital degrees of freedom in *d*-electron as well as *f*-electron systems have attracted much attention. In 4*f*-electron systems, strong intra-atomic spin-orbit coupling forces the orbital degrees of freedom to be described as quadrupole moments (rank-2 irreducible tensor operators of the total angular momentum *J*). The quadrupole moments often play an important role in forming exotic electronic ground states such as antiferroquadrupolar (AFQ) states with a staggered quadrupolar component and a non-Fermi liquid (NFL) state due to a two-channel (quadrupole) Kondo effect.

The Pr-based intermetallic compound $PrIr_2Zn_{20}$ crystallizes in the cubic $CeCr_2Al_{20}$-type structure with the space group Fd-3m and Z=8, where Pr atoms are encapsulated in the highly symmetric Frank-Kasper cages formed by 16 zinc atoms. We have recently reported that $PrIr_2Zn_{20}$ undergoes a superconducting transition at T_c=0.05 K [1]. The superconductivity was indicated by a large diamagnetic signal in the AC magnetic susceptibility. At T>30 K, the inverse magnetic susceptibility χ^{-1} follows the Curie-Weiss law, indicating the trivalent state of the Pr ions. On cooling below 30 K, χ^{-1} gradually approaches a constant value, characteristic of a Van-Vleck paramagnet. Furthermore, our analyses of the magnetic anisotropy in the paramagnetic state and a Schottky peak observed at around 10 K in the specific heat reveal that the crystalline electric field ground state of $PrIr_2Zn_{20}$ is the non-Kramers Γ_3 doublet with a magnetic Γ_4 triplet excited state lying at 30 K [2]. In order to reveal how the Γ_3 degeneracy is lifted at low temperatures, we extended the temperature range of the measurements of magnetization M and specific heat C down to 0.04 and 0.06 K, respectively.

In $C(T)$, a sharp peak appears at T_Q=0.11 K, indicating a phase transition. Since no magnetic anomaly was observed at around 0.11 K in $M(T)$, the origin of this phase transition is considered to be non magnetic. In magnetic fields, $C(T)$ shows the anisotropic responses. The B–T phase diagram for $\boldsymbol{B}$∥[100] and $\boldsymbol{B}$∥[110] is summarized in Fig. 1. Both the transition temperatures T_{Q1} ($\boldsymbol{B}$∥[100]) and T_{Q2} ($\boldsymbol{B}$∥[110]) increase in magnetic fields. This is a common feature in AFQ ordering systems. Therefore, this phase diagram provides evidence of an AFQ order in $PrIr_2Zn_{20}$. The superconducting transition was studied by AC magnetic susceptibility and electrical resistivity measurements. As shown in the inset of Fig. 1, the Meissner diamagnetic signal below 0.05 K fully compensates the opposite voltage of a reference superconductor $LaIr_2Zn_{20}$ (T_c=0.6 K) mounted in the counter part of a pickup coil [1]. The electrical resistivity goes down to zero at T_c. These confirm the bulk nature of the superconductivity in $PrIr_2Zn_{20}$. As displayed in the phase diagram, the superconducting state with T_c=0.05 K exists deep inside the AFQ ordered phase. Thus, $PrIr_2Zn_{20}$ is the first example in which a superconducting transition occurs in the AFQ phase. The 4*f* electronic entropy at T_Q reaches only 0.2Rln2 compared with Rln2 expected for the twofold degeneracy of the Γ_3 state. From these results, it is tempting to speculate that quadrupolar fluctuations might play an important role in the formation of the superconducting pairs. Further comprehensive studies using microscopic techniques would reveal the role of the quadrupolar degrees of freedom in superconductivity of $PrIr_2Zn_{20}$.

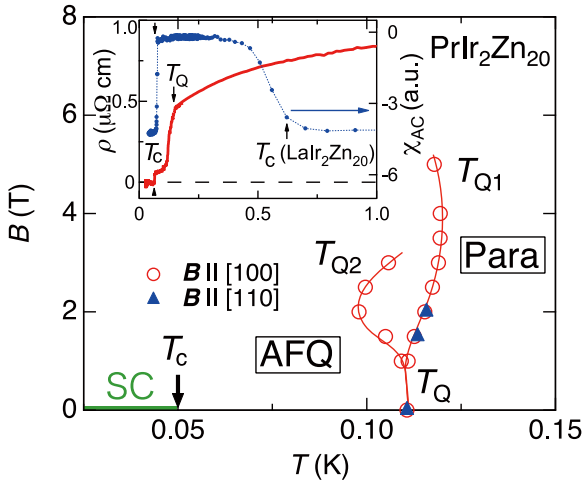

Fig. 1. B–T phase diagram of $PrIr_2Zn_{20}$ for $\boldsymbol{B}$∥[100] (open circles) and $\boldsymbol{B}$∥[110] (solid triangles). T_c and SC denote the superconducting transition temperature and the superconducting phase, respectively. The inset shows the temperature dependence of the AC magnetic susceptibility and the electrical resistivity.

References

[1] T. Onimaru, K. T. Matsumoto, Y. F. Inoue, K. Umeo, Y. Saiga, Y. Matsushita, R. Tamura, K. Nishimoto, I. Ishii, T. Suzuki, and T. Takabatake, J. Phys. Soc. Jpn. **79**, 033704 (2010).

[2] T. Onimaru, K. T. Matsumoto, Y. F. Inoue, K. Umeo, T. Sakakibara, Y. Karaki, M. Kubota, and T. Takabatake, Phys. Rev. Lett., **106**, 177001 (2011).

Authors

T. Onimaru[a], K. T. Matsumoto[a], Y. F. Inoue[a], K. Umeo[b], T. Sakakibara, Y. Karaki, M. Kubota, and T. Takabatake[a,c]

[a]AdSM, Hiroshima University

[b]N-BARD, Hiroshima University

[c]IAMR, Hiroshima Unversity

Magnetic Order in the Quasi-One-Dimensional Purely Organic Ferromagnet 2-BIMNN

T. Sugano and H. Mori

Organic and molecular magnets have recently become of great interest to physicists and chemists and can be expected to provide a wealth of opportunities for studying magnetic chains. This is because both the intrachain and interchain exchange interactions can be controlled, to some extent, using chemical modifications. Although there are many examples of spin 1/2 antiferromagnetic chains, the number of examples of spin 1/2 ferromagnetic chains is much smaller.

The nitronyl nitroxide route to organic magnetism is particularly attractive for synthesizing organic magnets since a variety of organic groups can be attached to the nitronyl nitroxide neutral radical in order to produce different crystal architectures which can favor or inhibit particular intermolecular interactions. We have focused on various substituted imidazolyl nitronyl nitroxides and identified the compound 2-benzimidazolyl nitronyl nitroxide (2-BIMNN, molecular structure shown in the inset to Fig. 2) which shows ferromagnetic interactions [1,2].

The neutral radical 2-BIMNN was prepared and characterized by measuring magnetization isotherms up to 7 T and magnetic susceptibility χ over the temperature range from 1.8 to 300 K. As reported elsewhere, susceptibility data above 70 K fit to a Curie-Weiss law with a Weiss constant θ = +17 K, indicating ferromagnetic interactions. A good fit

down to a few Kelvin is obtained using the one-dimensional Heisenberg ferromagnetic model (χ^{1d}) with an intrachain exchange constant J / k_B = 22 K. Below 5 K, χ exceeds χ^{1d}, but by introducing a ferromagnetic interchain coupling constant J', the data could be successfully fitted using the mean-field expression $\chi = \chi^{1d} / (1-2zJ'\chi^{1d} / Ng^2\mu^2_B)$ yielding $zJ' / k_B = +0.24$ K.

Our determined crystal structure (Fig. 1) is that the stacking of molecules along the *c*-direction, which provides relatively poor direct overlap between singly-occupied molecular orbitals on neighbouring molecules, favours ferromagnetic behavior in this compound. The quasi-one-dimensional nature of magnetic interactions is also observed in the angular dependences of the X-band electron spin resonance (ESR) linewidth of single crystal samples of 2-BIMNN. The angular dependences show maxima in B_{pp} whenever the applied field is parallel to the *c*-axis and minima at angles of ±54° (i.e. where $3\cos^2\theta - 1 = 0$).

Muon-spin rotation (μ^+SR) experiments can be particularly effective at identifying three-dimensional ordering in low-dimensional magnets since the signature of such ordering is unambiguous: a spontaneous precession of the muon spin-polarization observed in zero-field. This is in contrast to thermodynamic measurements, which are heavily dominated by the effect of intrachain interactions. Our μ^+SR experiments were carried out using the Low Temperature Facility (LTF) at the Swiss Muon Source, Paul Scherrer Institute, Switzerland. In our μ^+SR experiment, spin polarized positive muons (μ^+, momentum 28 MeV/*c*) were implanted into an array of very small crystals of 2-BIMNN. The muons stop quickly (in < 10^{-9} s), without significant loss of spipolarization. The observed quantity is then the time evolution of the average muon spin polarization $P_z(t)$, which can be inferred via the asymmetry in the angular distribution of emitted decay positrons, parameterized by an asymmetry function $A(t)$ proportional to $P_z(t)$.

Example μ^+SR spectra are presented in Fig. 2 and show that a clear precession signal is observed at low temperature, signifying the presence of long range magnetic order. The data are well described by the fitting function

$$A(t) = A_0 e^{-\Lambda t}\cos(2\pi\nu t + \phi) + A_1 e^{-\lambda t} + A_2 e^{-\sigma^2 t^2} + A_{bg} \qquad (1)$$

where ν is the muon precession frequency (equal to $\gamma_\mu B/2\pi$, with B the magnetic field at the muon site and $\gamma_\mu = 2\pi \times 135.5$ MHz T^{-1}) and A_{bg} is the background contribution from those muons that stop outside the sample. The first

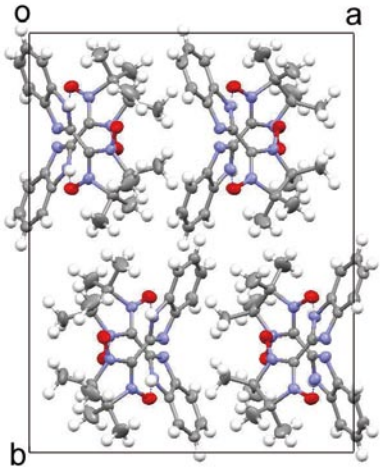

Fig. 1. The crystal structure of 2-BIMNN (2-benzimidazolyl nitronyl nitroxide) projected along the *c*-axis. The dotted lines show the dominant hydrogen bonds.

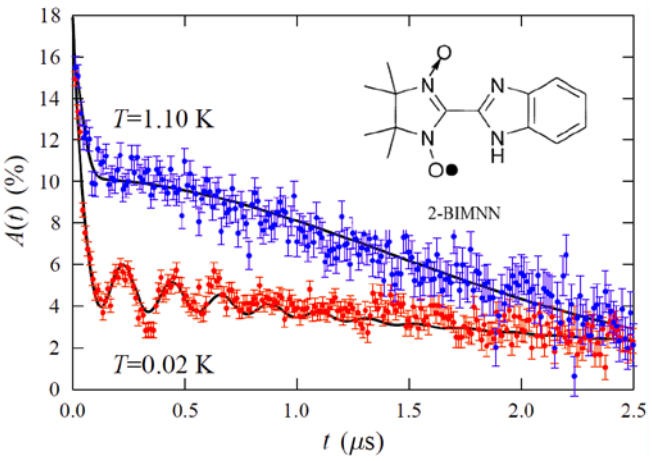

Fig. 2. μ^+SR spectra for 2-BIMNN measured above and below the magnetic transition at T_C = 1.0(1) K. Inset: the molecular structure of 2-BIMNN.

term, with amplitude A_0, arises from those muons that stop in positions of quasistatic magnetic order with their spin components perpendicular to the local magnetic field at the muon site (expected to be 2/3 of the total in a polycrystalline sample). The contribution with amplitude A_1 arises from the same muon sites but with muon-spin components oriented parallel to the local magnetic field (accounting for the remaining 1/3 of the signal). The ratio was found to be $A_0/A_1 \approx 2$ as expected for a polycrystalline material. The Gaussian signal with amplitude A_2, has a large relaxation rate at the lowest measured temperatures and probably arises from a class of muon sites with a range of large local magnetic fields. The observation of this large relaxing component is common in molecular materials, probably reflecting the variety of realized muon stopping states. Fits to Eq. (1) reveal the temperature evolution of the precession frequency. Above T = 0.6 K the large damping of the oscillating signal causes it to become unresolvable. However, the lack of any discontinuous change in either the shape of the relaxation or in the amplitudes of the components of the signal suggests that the ordering transition temperature is somewhat higher than T = 0.6 K. In fact the shape of the spectra changes more dramatically in the region $0.9 \le T \le 1.1$ K with the spectra measured for $T \ge 1.1$ K (Fig.2) taking the form of a low-amplitude, fast, initial relaxation which dominates the signal at early times superposed on a large-amplitude, slowly relaxing, Gaussian contribution. In fact, this is the typical $T > T_C$ spectrum observed in many molecular magnetic materials.

Our results on 2-BIMNN can be set in the context of other quasi-one-dimensional ferromagnets which have been discovered. The values of intrachain exchange constant is J, three-dimensional ordering transition temperature is T_c and the ratio is T_c / J. It is readily seen that 2-BIMNN is among the most strongly one-dimensional of the ferromagnetic chains and holds the record among purely organic magnets.

References

[1] T. Sugano, S. J. Blundell, W. Hays, and P. Day, Polyhedron **22**, 2343 (2003).
[2] T. Sugano, S. J. Blundell, T. Lancaster, F. L. Pratt, and H. Mori, Phys. Rev. B **82**, 180401(R) (2010).

Authors

T. Sugano[a], S. J. Blundell[b], T. Lancaster[b], F. L. Pratt[c], and H Mori
[a]Meiji Gakuin University
[b]Oxford University
[c] Rutherford Appleton Laboratory

Graphene π-Bands on Si-Terminated Vicinal SiC(0001)

S. Tanaka and F. Komori

Massless π bands of graphene grown on a SiC(0001) substrate can be modified by the scattering at the boundaries and the interface superstructure. We investigated the π band structure and width of the single- and double-layer graphene grown on a Si-terminated vicinal SiC(0001) substrate using angle-resolved photoemission spectroscopy (ARPES). The π electron scattering at the substrate steps makes the spectrum width anisotropic, but no difference in the π band shape. Quasi-2×2 replicas of the π band due to the interface $6\sqrt{3}\times6\sqrt{3}$-R30° superstructure were observed in the single-layer graphene while they were absent in the double-layer graphene.

Single- and double-layer graphenes were grown on Si-terminated surface of nitrogen-doped 6H-SiC(0001) substrates vicinal to the [11-20] (4°off) direction. [1] The substrate surface was first etched in H_2 gas, and a SiON thin film [2] was successively formed on the surface by annealing in N_2 gas. Finally, graphene layer was made on this substrate by annealing in N_2 gas over 1900 K for up to a few hundred sec. The average thickness of the graphene can be controlled by the annealing temperature and time. The STM images of the graphene are shown in Fig. 1. The graphene covers all the substrate including the step-edge areas.

Figure 2 shows the results of ARPES [3]. The π band spectrum in the direction perpendicular to the step-down direction (K_1) has a narrower width in the momentum distribution than the band in the other direction (K_2) when the binding energy from Fermi energy E_F is smaller than 0.2 eV. However, there is no significant difference in the π band shape between them. The anisotropy of the line width is attributed to the π electron scattering at the curved areas on the substrate step edges. The origin of the observed nonlinear dispersion of the π band is not due to the electron scatterings at defects of the graphene, but to the many-body effects and/or the electronic potential due to the interface $6\sqrt{3}\times6\sqrt{3}$-R30° structure of carbon atoms, which cause the quasi-2×2 replica π bands in ARPES.

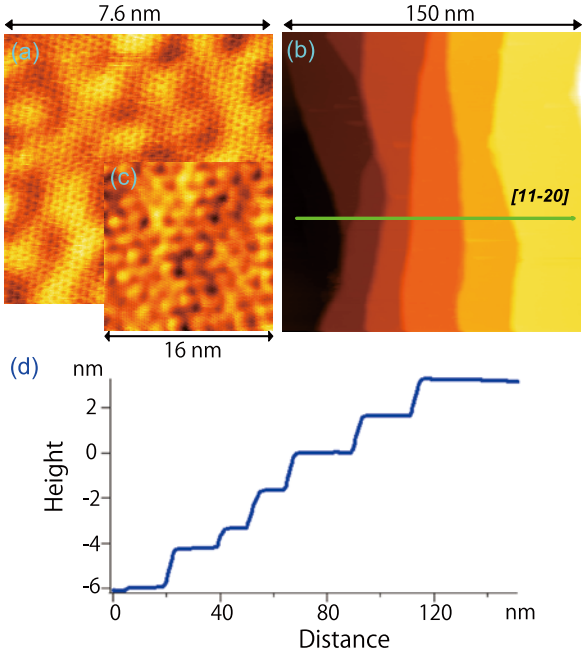

Fig. 1. (a-c) Topographic STM images of single-layer graphene grown on the Si-terminated SiC(0001) substrate vicinal to [11-20] direction. The hexagonal atomic arrangement and the interface $6\sqrt{3}\times6\sqrt{3}$-R30° superstructure can be seen for magnified images (a,c). A step-and-terrace structure is evident in the image of a wide area (b). The images were taken at 80 K. (d) Cross section along the line in (c).

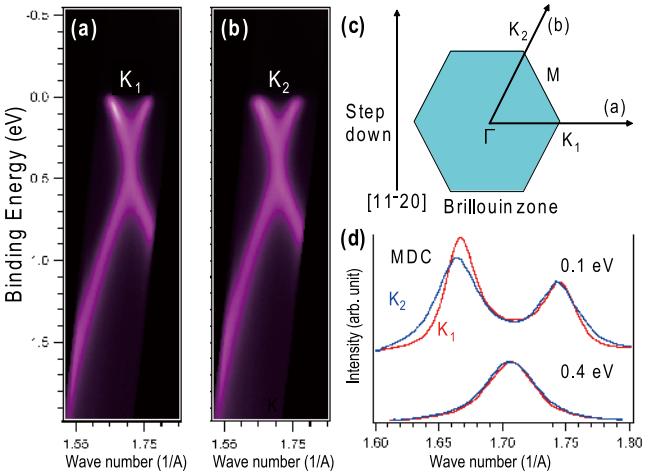

Fig. 2. (a,b) π band structures at two K points measured by ARPES for single-layer graphene grown on the SiC(0001) substrate vicinal to [11-20] direction. (c) Graphene Brillouin zone, and definitions of the K_1 and K_2 points. The Γ-K_1 direction is perpendicular to the step-down direction, and the Γ-K_2 direction is 30° rotated from the step-down direction. (d) Momentum distribution curves at 0.1 and 0.4 eV below E_F for the π band spectra around K_1 and K_2. At 0.1 eV, the line width around K_1 is narrower than that around K_2 while it is almost the same at 0.4 eV.

References
[1] S. Tanaka, *et. al.*, Phys. Rev. B **81**, 041406(R) (2010).
[2] T. Shirasawa, *et. al.*, Phys. Rev. Lett. **98**, 136105 (2007).
[3] K. Nakatsuji, *et. al.*, Phys. Rev. B **82**, 045428 (2010).

Authors
K. Nakatsuji, Y. Shibata, R. Niikura, K. Morita[a], S. Tanaka[a], F. Komori
[a]Kyushu University

Multilevel Resistive Switching at Oxide Interfaces

I. Ohkubo and M. Lippmaa

Band edge alignment at heterointerfaces between dissimilar oxides can result in new functional properties due to local changes in carrier density. Any accumulation or depletion layers that form at an interface, are usually static, determined by the dielectric properties and the Fermi level positions in the two materials on either side of an interface. In oxide heterostructures, an additional degree of freedom arises due to the presence of crystal defects, which are not necessarily static, but can be created or moved by an applied electric field, even at room temperature. It is thus, at least in principle, possible to change the effective doping levels in at an oxide interface after the crystal has been grown. The most straightforward way of probing such changes is to measure either the in-plane or transverse transport properties of an interface. As the process is in some cases reversible, there are also obvious memory device applications, where data is stored in a motion of ions, but probed by electronic transport. The presence of vacancies, dopants or other defects also leads to reversible defect level charging, which also affects cross-interface transport. A long-standing issue is the identification of the types of defect levels that form in the interface

layers and the depth of impurity or vacancy levels within the bandgap of insulating oxides.

In this collaborative project, our purpose is to study the formation of interface defects and identifying the defect level positions. The test material is a nm-order AlO_x thin film that is sandwiched between a metallic electrode and an insulating oxide, $(Pr,Ca)MnO_3$, which forms a suitable depletion layer at the AlO_x interface. The presence of charge at the defect sites is measured by looking at pulsed current flowing through the interface.

The essential parts of the structure used for the measurement are shown in Fig. 1. The heterostructure stack is grown on a $SrTiO_3$ substrate, which offers good lattice matching with the manganite layers. The bottom electrode of the junction is a metallic $La_{0.6}Sr_{0.4}MnO_3$ film, followed by an insulating 50 nm-thick $Pr_{0.8}Ca_{0.2}MnO_3$ layer. The actual depletion layer that we study forms at the interface between $Pr_{0.8}Ca_{0.2}MnO_3$ and AlO_x. Since there is a possibility of physically moving anion defects under high applied fields, the measurements are made by applying short 'write' pulses that inject or deplete charge at the interface. The change of accumulated charge at the interface affects the transport through the junction, and is probed by applying a low bias on the junction, while measuring current. In terms of device operation, this is known as a 'read' pulse. As shown in the switching resistance plot in Fig. 1, we can identify at least three stable resistance states in the heterostructure, corresponding to three charge states at the interface. A normal AlOx / $Pr_{0.8}Ca_{0.2}MnO_3$ interface normally shows two stable resistances, also known as the high resistance state and the low resistance state, corresponding to two conduction barrier heights that form at the interface. When the AlO_x film is doped with a transition metal impurity, in this case Co, an additional impurity level forms at the AlO_x layer. The presence of an additional impurity level is seen in the resistance behavior as the appearance of a third stable resistance state.

The approach used in this experiment can be extended to other dopant elements with different impurity level positions. It may thus be possible to use such impurity reference levels to identify the positions of intrinsic defects, such as aluminum or oxygen vacancies.

In addition to the ability to map the energy scales of defect levels in oxide heterostructures, resistive switching also has obvious applications in data storage. Intentional impurity doping can lead to memory architectures that can store more than one bit of information in a single memory cell.

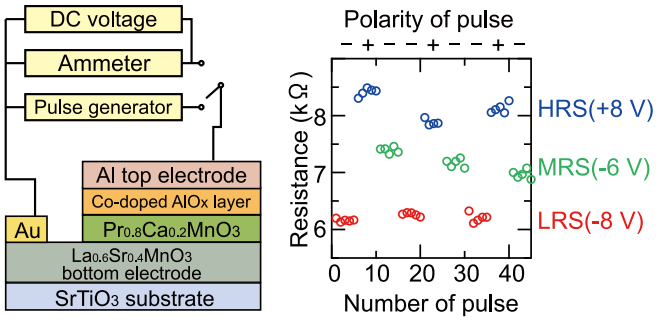

Fig. 1. (Left) Schematic device structure of a multivalue epitaxial manganese oxide-based resistive switching memory with an atomically engineered AlO_x interface barrier layer. The switching occurs in the barrier layer region. (Right) Pulsed write and read sequence showing reliable switching between three different resistance values.

Reference

[1] G. Sugano, I. Ohkubo, T. Harada, T. Ohnishi, M. Lippmaa. Y. Matsumoto, H. Koinuma and M. Oshima, Mat. Sci. Eng. B **173**, 3 (2010).

Authors

K. Tanigaki[a], I. Ohkubo[a], T. Harada[a], G. Sugano[a], K. Tsubouchi[a], M. Oshima[a], and M. Lippmaa

[a]Department of Applied Chemistry, University of Tokyo

Spin Current Manipulation in Superfluid ^{3}He A_1 Phase

A. Yamaguchi, Y. Aoki, and M. Kubota

The superfluid phases of liquid ^{3}He appear below a pressure-dependent transition temperature Tc. In zero applied magnetic field two superfluid phases known as A and B phases appear. In applied magnetic fields, a new A_1 phase emerges between the two transition temperatures T_{C1} and T_{C2} where $T_{C2} < T_C < T_{C1}$ at all pressures. The A_1 phase has been regarded as a "ferromagnetic" superfluid phase whose condensate involves spin polarized pairs with the energy gap $\Delta\uparrow\uparrow>0$ but $\Delta\downarrow\downarrow\equiv 0$. Such a unique phase like A_1 phase has not been observed in any other condensed-matter system yet. Therefore, it is quite interesting to investigate this magnetically ordered superfluid A_1 phase from the aspect of fundamental physics. The unique hydrodynamics of the A_1 phase originating in the broken relative spin-orbit-gauge symmetry allows spin superflow to be created either by magnetic field or pressure gradient; In the magnetic fountain effect (MFE), an applied magnetic field gradient across a superleak is accompanied by a pressure gradient, creating spin-flow through the superleak; In the mechano-spin effect (MSE), on

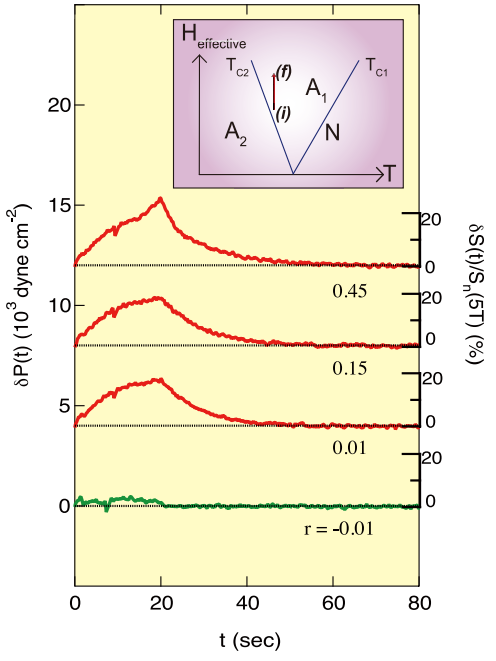

Fig. 1. MSE response in A_2 and A_1 phases (green and red curves, respectively). Temperatures are indicated by normalized reduced temperature $r = (T-T_{C1})/(T_{C1}-T_{C2})$. Induced spin-pressure differences (δP) (left ordinate) are plotted. δP for each r is displaced by 4000 dyne/cm^2 for clarity. The right ordinates show the computed fractional increase in spin-density difference $\frac{1}{2}\delta S/S_n$. The liquid pressure is 28 bar and the applied static magnetic field is 5 T. Inset: Phase diagram of superfluid ^{3}He at a constant liquid pressure. The MSE process corresponds to the red arrow.

the other hand, the mechanically applied pressure gradient, and the superleak serving as spin filter, enable us to directly create spin supercurrent and to boost spin polarization of ^{3}He in a small chamber. Recently, we have extensively studied on the spin fluid dynamics in the A_1 phase using both the MFE and MSE techniques [1-5]. One very important issue in the spin fluid dynamics is the origin of the unexpected spin relaxation that we observed in MFE experiments [1]. Understanding this spin relaxation would yield important clues in designing a spin-pumping device for boosting the spin polarization to much greater level than feasible by available static magnetic fields.

So far, the MSE experiments have been carried out to observe the accumulated spin density in the small chamber by using a glass capillary array (to increase the spin/mass flux) as the superleak and a flexible membrane as an electrostatically actuated pneumatic pump [4]. The change in spin density was deduced from the measured differential pressure. Measurements in an applied static magnetic field of 5 T indicate that the superfluid polarization increases by 20 ~ 50% from that produced by the static field (Figure 1). That is, the effective field increased to 6 ~ 7.5 T. Remarkably, even a tiny electrical voltage of several hundreds volts applied to the actuator, exerts a tesla-scale effecitive field on the system. The increase in polarization is corroborated by the observed increase in the spin relaxation time. By making improvements in (1)superleak, (2)decreasing the chamber volume and (3)improving the pneumatic pumping mechanism, even greater increase in polarization should be possible.

We are currently developing a new ^{3}He -hydraulic actuator for achieving greater enhancement of spin density. The actuator consists of two small liquid ^{3}He chambers located at a 4.2 K plate and in the interior of the cell. The pressure in the 4.2 K chamber is heater-controlled and it transmits a force onto a flexible membrane in the cell. The motion of the membrane induces spin-polarized current through an array of superleak capillary tubes into an accumulation chamber. At the same time, a high field-^{3}He-NMR detector is tested to detect the polarization increase directly.

The superfluidity of liquid ^{3}He in the higher magnetic fields is one of the long-standing unexplored topics in the ultra-low temperature physics. It might open up a new technique for manipulating the spin super current and for studying A_1 phase in much greater effective field than the maximum 15 T static field so far achieved.

References

[1] A. Yamaguchi, S. Kobayashi, H. Ishimoto, and H. Kojima, Nature, **444**, 909 (2006).
[2] A. Yamaguchi, S. Kobayashi, H. Ishimoto, and H. Kojima, J. Low Temp. Phys., **148**, 513 (2007).
[3] A. Yamaguchi, Y. Aoki, K. Suzuki, H. Ishimoto, and H. Kojima, J. Phys.: Conf. Ser. **150**, 032122 (2009).
[4] A. Yamaguchi, Y. Aoki, S. Murakawa, H Ishimoto, and H. Kojima, Phys. Rev. B **80**, 052507 (2009).
[5] Y. Aoki, A. Yamaguchi, K. Suzuki, H. Ishimoto, and H. Kojima, Phys. Rev. B **82**, 054527 (2010).

Authors

A. Yamaguchi[a], M. Wada[a], G. Motoyama[a], A. Sumiyama[a], Y. Aoki[b], Y. Okuda[b], S. Murakawa[c], Y. Karaki, M. Kubota, and H. Kojima[d]

[a]The University of Hyogo
[b]Tokyo Institute of Technology
[c]Keio University
[d]Rutgers University

Pressure Induced Valence Transition of $EuCo_2P_2$

T. Nakama, M. Hedo, and Y. Uwatoko

The rare-earth (R) transition metal (T) phosphides, RT_2P_2, which crystallize in the $ThCr_2Si_2$-type body-centered tetragonal structure, have a rich variety of the magnetic ground states such as 4*f* sub-lattice magnetism, 3*d* sub-lattice magnetism or magnetism of both sub-lattices [1-3]. In this series, $EuCo_2P_2$ is an antiferromagnet with a moment at Eu site of 6.9 μ_B and the Neel temperature of T_N = 66.5 K at ambient pressure. It is reported that $EuCo_2P_2$ undergoes a structural and magnetic phase transition at a pressure of P_c ~ 3 GPa from a long P-P distance phase, with magnetic Eu^{2+} and nonmagnetic Co, into a short P-P distance phase with nonmagnetic Eu^{3+} and magnetic Co with an estimated moment of 0.6 μ_B at the Co site [4,5]. Thermopower *S* and resistivity ρ were measured simultaneously at temperatures from 2 K to 300 K on the process of applying pressure [6].

Figure 1 shows the temperature dependence of *S* under pressures up to 2 GPa. At ambient pressure, *S* increases with increasing temperature, having a maximum around 60 K and a break at T_N ~ 66 K. With increasing pressure, *S* deceases in the whole measuring temperature range and T_N increases in the pressure range of P < 2.0 GPa. The inset of Fig. 1 shows the temperature dependence of *S* at 2.5 and 3.0 GPa. The temperature variation of *S* shows a dramatic change at the critical pressure P_c. No characteristic feature accompanied by the magnetic phase transition in the high pressure phase is observed in $S(T)$, as shown in the inset of Fig. 1. Since the large DOS mainly due to the 3*d* states lies near the Fermi level [4,7], the transport properties of $EuCo_2P_2$ are strongly depend on the state of the Co 3*d* electrons. Then, it is considerable that the drastic changes of the features of $S(T)$ and $\rho(T)$, but is not shown in this report [8], at P_c indicate a large modification of the 3*d* electronic state around the Fermi level due to a pressure induced structural and magnetic phase transition, which should be connected with a difference between the variations of *S* and ρ at the magnetic phase transition temperature in the low pressure phase and those in the high pressure phase.

Figure 2 indicates the pressure dependence of the

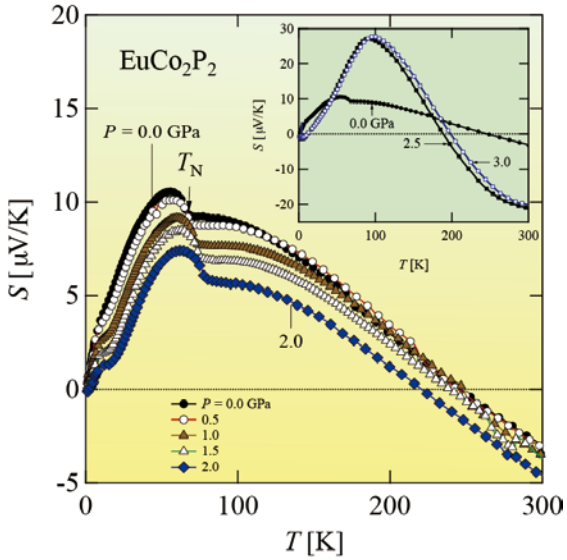

Fig. 1. Temperature dependence of *S* of $EuCo_2P_2$ under pressures up to 2 GPa. The inset shows the temperature dependence of *S* at P = 2.5 and 3.0 GPa.

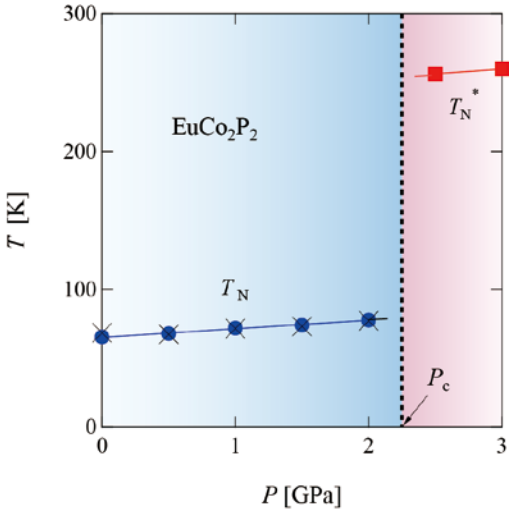

Fig. 2. Pressure dependence of the magnetic phase transition temperatures T_N in the low pressure phase and T_N* in the high pressure phase. The symbols of ● and × in the low pressure phase are obtained from ρ(T) and S(T) curves, respectively. The data in the high pressure phase ■ is obtained from ρ(T) [8]. The solid lines are guides for the eye.

magnetic phase transition temperatures, T_N in the low pressure phase and T_N* in the high pressure phase. T_N increases with increasing pressure, dT_N /dP ~ 6 K/GPa, and shows a discontinuous jump at the critical pressure P_c, indicating the first order phase transition from the low pressure phase, with the magnetic Eu^{2+} and nonmagnetic Co, into the high pressure phase with nonmagnetic Eu^{3+} and magnetic Co [5]. T_N* in the high pressure phase slightly increases with increasing pressure.

References
[1] M. Reehuis *et al.*, J. Phys. Chem. Solids **53**, 687 (1992).
[2] E. Morsen *et al.*, J. Phys. Chem. Solids **49**, 785 (1988).
[3] M. Reehuis *et al.*, J. Phys. Chem. Solids **54**, 469 (1993).
[4] B. Ni *et al.*, Phys. Rev. B **63**, 100102(R) (2001).
[5] M. Chefki *et al.*, Phys. Rev. Lett. **80**, 802 (1998).
[6] M. Hedo *et al.*, J. Phys.:Conf. **215**, 012186 (2010).
[7] P. H. Andersson *et al.*, Phys. Rev. B **65**, 174109 (2002).
[8] T. Nakama *et al.*, J. Phys.:Conf. **200**, 032050 (2010).

Authors
T. Nakama[a], T. Yoshida[a], A. Ohno[a], D. Nakamura[a], Y. Takaesu[a], M. Hedo[a], K. Yagasaki[a], K. Uchima[b], T. Fujiwara[c], T. Shigeoka[c], K. Matsubayashi and Y. Uwatoko
[a]University of the Ryukyus
[b]Okinawa Christian Junior College
[c]Yamaguchi University

Electronic Signature of Hidden Order in URu_2Si_2

R. Yoshida, T. Yokoya, and S. Shin

The heavy fermion material URu_2Si_2 exhibits superconductivity (T_c ~1.5 K) and mysterious second-order phase transition at ~17.5 K (T_{HO}). The latter order is characterized by a large entropy release, and clear anomalies have been found at the ordering temperature in various bulk measurements. However, microscopic nature of the order has not been detected, and even today, the order parameter as well as the ordering vector of this phase transition is still yet-to-be determined. This is known as the 'hidden-order' problem today, and the possibility of new-type second-order phase transition is anticipated.

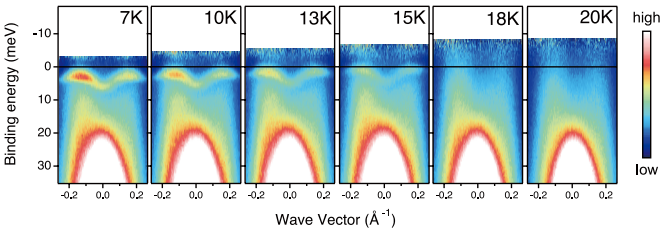

Fig. 1. False-color ARPES intensity maps of URu_2Si_2 taken at temperatures above and below the hidden order transition. Note that intensity maps represent band dispersion along (π, 0) direction. A narrow dispersive feature is observed near the Fermi level only in the hidden-order state.

Although a number of experimental studies are currently available on URu_2Si_2, there has been no spectroscopic data for a long time that provides the direct information on the evolution of electronic structure across the hidden order transition. In fact, earlier photoemission experiments on URu_2Si_2 only studied the paramagnetic phase owing mainly to achievable energy resolution and cooling capability of spectrometers at that time. Recently, scanning tunneling spectroscopic studies and angle-resolved photoemission (ARPES) studies have revealed the change of electronic states near the Fermi level at the transition temperature. Here, we present our data on URu_2Si_2 obtained by laser ARPES, focusing on the temperature dependence of spectral function near the Fermi level [1].

In Figure 1, we show false-color ARPES intensity maps near the Fermi level obtained for (100) direction of URu_2Si_2. Note that the intensity maps are normalized by the resolution-convoluted Fermi functions. At all investigated temperatures, we observe the surface state and the hole-like dispersion. However, at temperatures above T_{HO} (18 – 25 K), no other feature is observed. On the other hand, at temperatures below T_{HO} (7 – 15 K), the narrow dispersive band appears near the Fermi level. This narrow dispersive band shifts to higher binding energies, and its spectral intensity increases as temperature is lowered. We also carry out ARPES measurements on $U(Ru_{1-x}Rh_x)_2Si_2$ (x ~ 0.03) where the band dispersion is measured for (100) direction. For Rh concentration of x ~ 0.03, the substitution of Rh for Ru is known to suppress the hidden order phase almost completely and to induce antiferromagnetic phase. The ARPES data taken at 7 K shows the surface state and the hole-like band, and these features are also present in the intensity map obtained at 26 K. However, we do not observe any signature of the narrow dispersive feature at all.

From the temperature dependence of the narrow dispersive band and its absence in Rh-doped sample, we conclude that the appearance of the narrow band must be a clear signature of the hidden-order transition. Moreover, our data shows that the narrow band appears only below T_{HO} and its spectral weight enhances as temperature is lowered. This behavior not only suggests the modification of band structures but also reveals that the change is not restricted to the immediate vicinity of the Fermi vector. One of the most natural interpretations of our data is to invoke the change of electronic periodicity upon the hidden-order transition. Then, the appearance of a new band at the onset of phase transition is reasonably explained by the backfolding of the band.

Reference
[1] R. Yoshida, Y. Nakamura, M. Fukui, Y. Haga, E. Yamamoto, Y. Onuki, M. Okawa, S. Shin, M. Hirai, Y. Muraoka, and T. Yokoya, Phys. Rev. B **82**, 205108 (2010).

Authors
R. Yoshida[a], Y. Nakamura[a], M. Fukui[a], Y. Haga[b], E. Yamamoto[b], Y. Onuki[b, c], M. Okawa, S. Shin, M. Hirai[a], Y. Muraoka[a], and T. Yokoya[a]
[a]Okayama University
[b]Japan Atomic Energy Agency
[c]Osaka University

Development of Three-Dimensional Scanning Photoelectron Microscope at the University-of-Tokyo Materials Science Outstation Beamline SPring-8 BL07LSU

K. Horiba, H. Kumigashira, and M. Oshima

With the evolution of nanotechnology, nanoscale analyses of device structures and self-assembled structures are greatly required. In particular, it is important to investigate the nanoscale distribution of electronic structures and chemical states along depth as well as lateral directions in order to understand the mechanisms and characteristics of complicated nanostructure species such as stacking structures in semiconductor devices and the surface/interface reactions of catalytic materials. Here, we report a newly developed scanning photoelectron microscope (SPEM) system with a depth profiling analysis capability for three-dimensional (3D) spatially resolved electron spectroscopy for chemical analysis (ESCA) of solids. We call this system "3D nano-ESCA." The system has been installed at the University-of-Tokyo Materials Science Outstation beamline, BL07LSU, at SPring-8.

The concept of 3D nano-ESCA is illustrated in Fig. 1. A SR X-ray beam is focused to nanometer size on the samples using a Fresnel zone plate (FZP). We use a 200 μm-diameter FZP with an outermost zone width of 35 nm. We can obtain lateral (x and y) distribution of photoelectron spectra by scanning the samples along the lateral directions and acquiring the photoelectron spectrum at each point. This is the typical scheme of SPEM. In addition to SPEM measurements, we simultaneously detect the angular distribution of emitted photoelectrons using an angle-resolved photoelectron spectrometer. In order to achieve high energy-resolution and a wide acceptance angle, a modified spherical photoelectron spectrometer with a two-dimensional (energy and angular distributions) detector and an extremely wide-angle

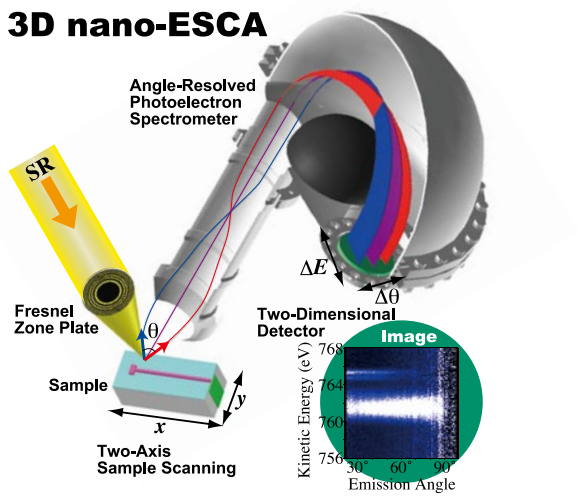

Fig. 1. Conceptual scheme of 3D nano-ESCA system.

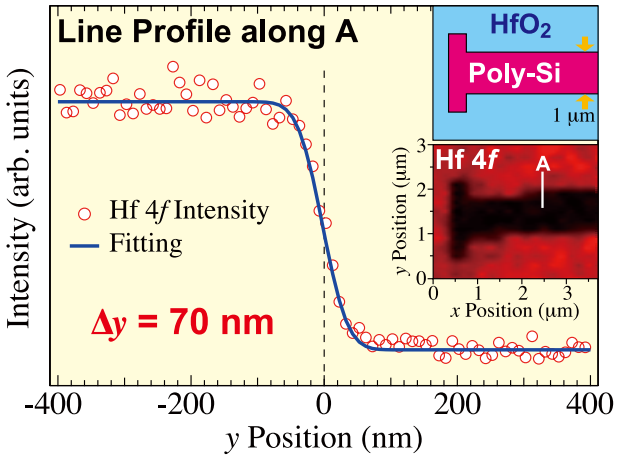

Fig. 2. Estimation of the spatial resolution from the line profile at the edge of the gate pattern along line A in the inset of the figure. The inset shows a schematic view of nano-patterned poly-Si electrodes on HfO_2 films and Hf 4*f* photoelectron-intensity mapping of the nano-patterned poly-Si/HfO_2 structure, obtained at the excitation photon energy of 870 eV.

lens with the acceptance angle of 60° is adopted. The angular distribution corresponds to the probing-depth dependence of the photoelectron spectra and can be converted into the depth profiling z information using maximum-entropy methods. Thus, we can obtain three-dimensional x, y, and z distribution of the electronic structure and chemical bonding states of the samples on a nanometer scale.

For demonstrating the capability of our system, we carried out SPEM measurements on nano-patterned poly-Si gate electrodes fabricated on HfO_2 films. The line profile of Hf 4*f* core-level photoelectron intensity at the edge of the gate pattern in Fig. 2 is fitted using a step function convoluted with a Gaussian function, and the full width at half maximum of the Gaussian function under the best-fit condition is determined to be 70 nm. Therefore, we have confirmed that the spatial resolution better than 70 nm is achieved.

References

[1] K. Horiba, Y. Nakamura, N. Nagamura, S. Toyoda, H. Kumigashira, M. Oshima, K. Amemiya, Y. Senba, and H. Ohashi, submitted to Rev. Sci. Instrum.
[2] M. Oshima, S. Toyoda, H. Kamada, T. Tanimura, Y. Nakamura, K. Horiba, and H. Kumigashira, ECS Trans. **33**, 231 (2010).
[3] S. Toyoda, Y. Nakamura, K. Horiba, H. Kumigashira, M. Oshima and K. Amemiya, e-J. Surf. Sci. and Nanotech. **9**, 224 (2011).

Authors
K. Horiba[a,b,c], Y. Nakamura[a], N. Nagamura[a], S. Toyoda[a], H. Kumigashira[a,b,d], M. Oshima[a,b,c], K. Amemiya[c,e], Y. Senba[f], and H. Ohashi[f]
[a]Department of Applied Chemistry, the University of Tokyo
[b]Synchrotron Radiation Research Organization, the University of Tokyo
[c]Core Research for Evolutional Science and Technology
[d]Precursory Research for Embryonic Science and Technology
[e]High Energy Accelerator Research Organization
[f]SPring-8

Shape Deformation and Phase Separation Dynamics of Two-Component Vesicles

T. Taniguchi and H. Noguchi

Recently, Sakuma *et al* [1] have reported that a single pore is formed by changing of temperature in two-component

vesicles composed of cone-like lipid (DHPC) and cylinder-like lipid (DPPC). They found a very novel phenomenon that the membrane on periphery of the pore rolls toward outside of the vesicle in a certain range of composition. We proposed a model to describe the shape deformations of the DHPC/DPPC binary vesicle after forming a single pore. After forming a single pore, the total free energy of the vesicle with coexisting fluid domains is given as $F=F_b+F_{mix}+F_{rim}$. F_b is the bending energy. F_{mix} is the mixing free energy including the line energy at domain boundaries, in each of two leaflets of bilayer membrane. F_{rim} is the energy of rim of membrane with a pore. For the vesicle with a pore, the area difference energy can be omitted, since the lipids can be exchanged through the capped rim at the pore of the vesicle. The dynamics of shape deformation is assumed to be described by relaxation type equation [2] where we used a local Lagrange multiplier to guarantee the local incompressibility condition for membrane area. It should be noted that the pore formation breaks the conservation law of vesicle volume and the mass conservation of each component in each inner and outer leaflets. The time evolutions of the local composition of DHPC in the inner and outer leaflets are given by diffusion type equations describing diffusions of DHPC lipids driven by the thermodynamic force and a transport of DHPC lipids between the inner and outer leaflets through the capped rim. Although the equilibrium shapes of two-component vesicle have been intensively investigated theoretically and numerically, none of these investigations has reported a membrane with a rolled rim. Therefore, in order to describe the dynamics of shape deformation and phase separation of two-component vesicle with a single pore and to understand the reason why the membrane can be rolled near the rim after forming a pore, we consider

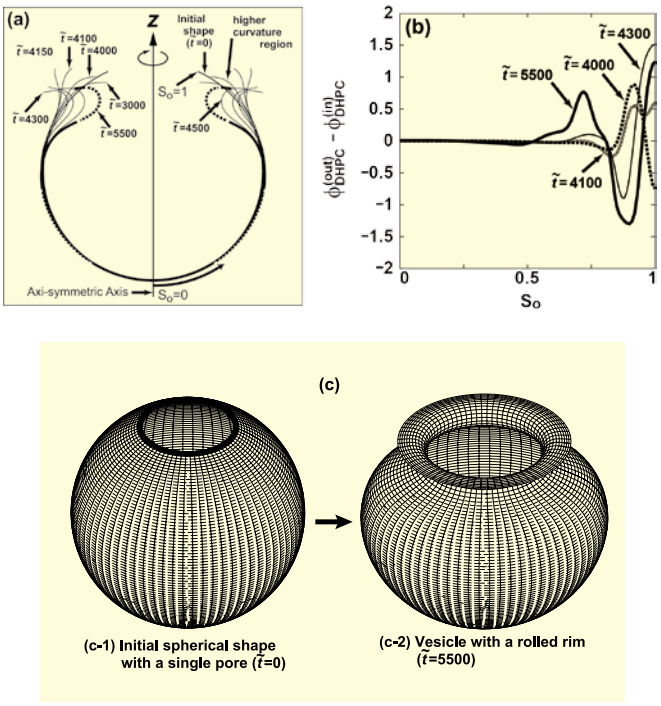

Fig. 1. (a) Cross section of the vesicle with a single pore as a function of dimensionless time $\tilde{t}$. A rolled-rim formation can be seen at around $\tilde{t}$ =5500. (b) Time evolution of the volume fraction difference, $\phi^{(out)}_{DHPC} - \phi^{(in)}_{DHPC}$, in DHPC between the inner and outer leaflets along the surface coordinate s_o. The depletion region is formed at around $s_o \cong 0.85$ in $\tilde{t}$ =5500. (c) Three dimensional view of the vesicle shape at the initial state and at $\tilde{t}$ =5500. The rolled-rim structure is formed well at $\tilde{t}$ =5500.

the model mentioned above. The highlight of our newly proposed model is the incorporation of two new contributions, (i) transfer of lipids through the cap at the rim and (ii) stabilization of the pore by the cone shape lipid into the previous continuum model. In this work, we considered an axi-symmetric spherical vesicle with a single pore which is assumed to be the state just after bursting, and we investigated numerically the shape deformation and phase separation dynamics using the model of two-component membrane. It is found from the numerical simulations that our model well reproduces the vesicle shape with a rolled rim as shown in Fig. 1. We also found that the origin of rolled rim is the formation of depletion of DHPC in the outer leaflet near the rim of pore coming from the phase separation induced by the edge energy at the rim.

References
[1] Y. Sakuma *et al.,* Biophysics Journal, **99**, 472 (2010).
[2] T. Taniguchi *et al.*, J. Phys.: Condens. Matter (to be published).

Authors
T. Taniguchi[a] and H. Noguchi
[a]Kyoto University

Numerical-Diagonalization Study of Spin Gap Issue of the Kagome-Lattice Antiferromagnet

H. Nakano and T. Sakai

Kagome-lattice antiferromagnet is a fundamental system with magnetic frustration. In spite of extensive studies, our understanding of this system is not sufficient due to the limitation of effective methods of analysis. One of the unresolved issues of this system is whether or not there exists a spin gap, namely a singlet-triplet energy gap.

For such a two-dimensional frustrated system as the kagome-lattice antiferromagnet, it is considered that the numerical-diagonalization method is effective; this method is widely used in various studies. However, more than ten years have been passed since numerical-diagonalization results of the kagome-lattice system with 36 sites were reported [1,2] unless calculations of larger systems have been successfully carried out. This situation prevents us to understand properties of the infinitely large system deeply. Under the circumstances, we have successfully carried out numerical diagonalization of the systems with 39 sites and 42 sites by large-scale *parallel* calculations. The largest calculations were carried out in an MPI-parallelized job with 8192 processes in the supercomputer, SGI Altix ICE 8400EX, ISSP, University of Tokyo. It is noticeable that the dimension of the largest matrix is d=538,257,874,440, which has become a new world record in successful numerical-diagonalization calculations. In addition, our study has become the first report that presents a finite-size energy difference of spin excitation for a 42-site system among S=1/2 spin models.

Using these results, we study the system-size dependence of the singlet-triplet energy gap of finite-size kagome-lattice systems [3]. Figure 1(A) shows an extrapolation analysis in the plot of the gap vs. $1/N_s$ under the assumption of presence of a nonzero spin gap, where N_s denotes the number of spin sites. One can observe two sequences of even-N_s and odd-N_s. In spite of the fact that both the sequences are supposed to

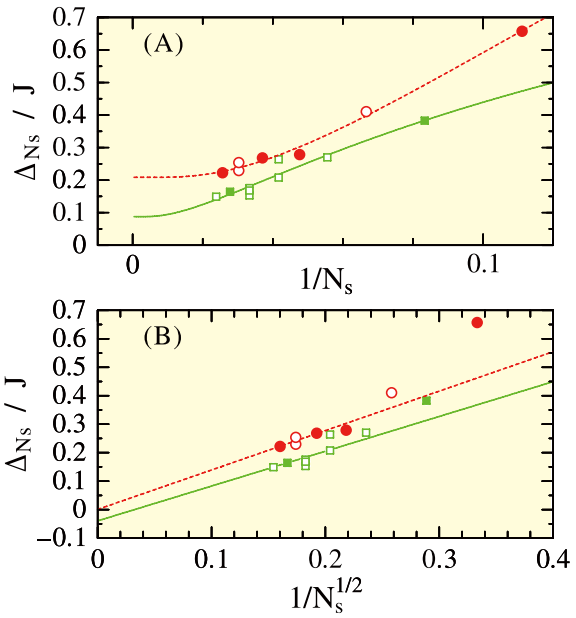

Fig. 1. Extrapolation of the singlet-triplet energy difference of the finite-size systems of kagome-lattice antiferromagnet. The essential difference between the two plots (A) and (B) is the scale of the axis of abscissa. Red circles and green squares denote data of even and odd N_s; curves and lines are drawn as results of fitting of data in the corresponding colors. Closed symbols mean that the clusters are rhombic; open symbols mean that they are not. Curves in (A) are consequences from the fitting under the assumption of nonzero gap; the disagreement of the two extraploated values from even- and odd-N_s data indicates the failure of the analysis. Lines in (B) are fitting lines under the assumption of absence of such a gap; the intersections of the two lines with the axis of ordinate indicate that the system is gapless.

share the common value in the thermodynamic limit, the extrapolated results from the two sequences differ from each other. This disagreement means that the assumption of the presence of a nonzero energy gap is invalid. On the other hand, we examine an extrapolation analysis under the assumption of absence of a nonzero spin gap in the plot of the gap vs. $1/N_s^{1/2}$, which is shown in Fig. 1(B). This plot is related to a linear dispersion relation of a system with a long-range order. The linear fitting reveals being gapless in the thermodynamic limit as a common consequence from the even-N_s and odd-N_s sequences.

Our theoretical consequence of the gapless spin excitation of the kagome-lattice antiferromagnet is in agreement with the fact that no spin gap is observed experimentally [4]. This study will be followed by the examination of whether or not the long-range order exists. Numerical-diagonalization calculations of systems as large as possible will provide us with a new and better understanding of condensed-matter physics.

References

[1] P. Lecheminant, B. Bernu, C. Lhuillier, L. Pierre, and P. Sindzingre, Phys. Rev. B **56**, 2521 (1997).
[2] Ch. Waldtmann, H.-U. Everts, B. Bernu, C. Lhuillier, P. Sindzingre, P. Lecheminant and L. Pierre, Eur. Phys. J. B **2**, 501 (1998).
[3] H. Nakano and T. Sakai, J. Phys. Soc. Jpn. **80**, 053704 (2011).
[4] P. Mendels and F. Bert, J. Phys. Soc. Jpn. **79**, 011001 (2010).

Authors
H. Nakano[a] and T. Sakai[b]
[a]University of Hyogo
[b]Japan Atomic Energy Agency, SPring-8

Superparamagnetism Induced by Polar Nanoregion in Relaxor Ferroelectrics Having Magnetic Ions

M. Soda, Y. Wakabayashi, and K. Hirota

Since multiferroic activity was discovered in a perovskite-type manganite $TbMnO_3$ in 2003, multiferroic materials attract great interest of researchers in the fields of materials science and condensed matter physics. The origin of the ferroelectricity in the multiferroic material has been discussed by several theory groups and so-called spin current model was turned out to explain most of the multiferroicity realized in screw type antiferromagnet. Experimentally, the control of the electric polarization by external magnetic field or of the magnetization by external electric field is the center of interest. Although multiferroic systems induced by non-trivial-magnetic structures are prevailing, it is also important to explore other origins of ME effects or the correlation between the dielectric property and magnetism. To this end, we studied a relaxor ferroelectrics having magnetic ions, which involves randomly oriented very local polar nanoregions (PNRs), $2/3BiFeO_3$-$1/3BaTiO_3$ (BFO-1/3BTO). In the present study, the interaction between the PNR and magnetism were studied both by macroscopic property measurements and microscopic neutron-scattering measurements on single crystalline sample of BFO-1/3BTO that reveals a new class of superparamagnetism induced by PNR.

In the neutron studies of BFO-1/3BTO, magnetic reflections at the ***Q***-points ($h'/2,h'/2,l'/2$) (h' and l' are odd), which are originated from G-type antiferromagnetic order, were observed at low temperatures. Although the system has the simple G-type magnetic structure, the T-dependence of the magnetic reflection is not simple. The T-dependences of the magnetic correlation length estimated from 1/2 1/2 1/2 magnetic peak profiles are shown in Fig. 1(a) with open circles. This indicates that the magnetic correlation is not long-ranged in the wide temperature region. Around 500 K, the magnetic correlation length approaches 8 nm as T increases. To examine the dielectric properties, nuclear diffuse scattering was also measured. The PNR, which is related to the relaxor property, induces nuclear diffuse scattering for typical relaxors. The nuclear correlation length, estimated from the profile width of the nuclear diffuse scattering, is plotted in Fig. 1(a) against T with closed circles. The size of PNRs is about 8 nm in a wide temperature region.

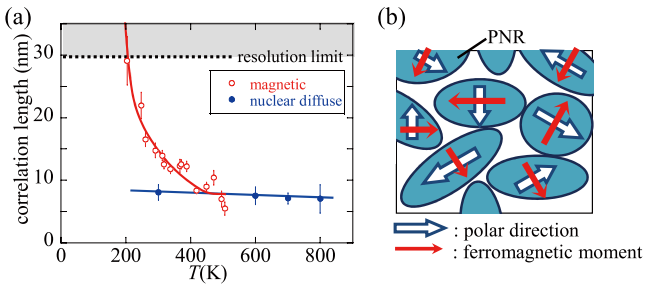

Fig. 1. (a) Temperature dependence of the correlation lengths in BFO-1/3BTO. Open and closed circles indicate the magnetic and the nuclear correlation lengths, respectively. (b) Polar nanoregions (PNRs) and nano-magnetic domains induced by the PNRs. In the polar region, the inversion symmetry is broken and Dzyaloshinskii-Moriya interaction works. The cant moment should be perpendicular to the polarization direction. The in-plane freedom of the magnetic ordering direction as well as the eight equivalent <111> directions allow the magnetic flexibility required for superparamagnetism.

From these neutron results, we propose that the G-type antiferromagnetic order is suppressed by PNRs and their domain walls, which are associated with the randomness of the crystal structure. The PNR size estimated by the nuclear diffuse scattering is 8 nm, and the magnetic correlation length also approaches 8 nm at around 500 K as T increases. These results mean that the magnetic correlation is limited within a PNR above 200 K. As T decreases, the magnetic correlation between neighboring PNRs begins to grow gradually. Since PNRs and their domain walls are the origins of the short-range order, significant suppression of the antiferromagnetic order was observed in BFO-1/3BTO, which has PNR.

When tiny magnetic particles are collected, superparamagnetic behavior is expected. Such magnetic property was actually observed in BFO-1/3BTO. The size of the magnetic particle, estimated from the superparamagnetic magnetization curve, coincides with the size of the PNR. The ferromagnetic component was originated from the cant of the Fe moments, which is induced by PNR having the rhombohedral distortion through the Dzyaloshinskii-Moriya interaction, as shown in Fig. 1(b). Since the same domain structure provides both electric and magnetic properties, strong coupling between the two properties through the domain size is expected.

Reference

[1] M. Soda, M. Matsuura, Y. Wakabayashi, and K. Hirota, J. Phys. Soc. Jpn. **80**, 043705 (2011). (Papers of Editors' Choice)

Authors

M. Soda[a,b], M. Matsuura[c], Y. Wakabayashi[b], and K. Hirota[b]

[a]University of Tokyo

[b]Osaka University

[c]Tohoku University

High-Field Magnetization of $CeOs_2Al_{10}$

T. Nishioka, M. Sera, and K. Kindo

CeT_2Al$_{10}$ (T = Ru, Os, Fe) have recently attracted much attention because of their unusual physical properties. These compounds belong to the category of the Kondo semiconductor. The most characteristic feature in this system is that $CeRu_2Al_{10}$ and $CeOs_2Al_{10}$ exhibit an unusual long-range order. Among CeT_2Al$_{10}$ compounds, $CeRu_2Al_{10}$ is most intensively studied. At the early state, although the nonmagnetic transition was proposed [1-3], the neutron scattering revealed that the antiferro-magnetic (AFM) order occurs at T_0 = 27.3 K in $CeRu_2Al_{10}$ [4]. The AFM order is characterized by an AFM moment (M_{AF}) of ~ 0.34 μ_B/Ce parallel to the c axis. Although it is now confirmed that the magnetic ordering with M_{AF} // c is realized below T_0, the magnetic ordered state is definitely not a simple one and there exist many unusual properties; a very high T_0 despite a small ordered moment, no metamagnetic transition despite the existence of a large spin gap without a low energy magnetic excitation [5], the magnetic order with M_{AF} // c even though the magnetic susceptibility along the a axis (χ_a) is much larger than χ_c in the paramagnetic region [1, 3].

$CeOs_2Al_{10}$ exhibits physical properties similar to those of $CeRu_2Al_{10}$ and the same type of magnetic order is expected to be realized below T_0 [1, 6]. On the other hand, there exist the following differences. T_0 is equal to 28.7 K which is a little higher than that of $CeRu_2Al_{10}$, the magnetic entropy released at T_0 and the magnitude of the ordered moment are smaller than those in $CeRu_2Al_{10}$, χ_a and χ_c in the paramagnetic region exhibit a broad maximum at T_{max} ~ 40 K in $CeOs_2Al_{10}$, the spin gap energy is 11 meV [7] which is higher than 8 meV in $CeRu_2Al_{10}$ [5]. To clarify the origin of the above differences between the two compounds, we measured the high field magnetization of $CeOs_2Al_{10}$.

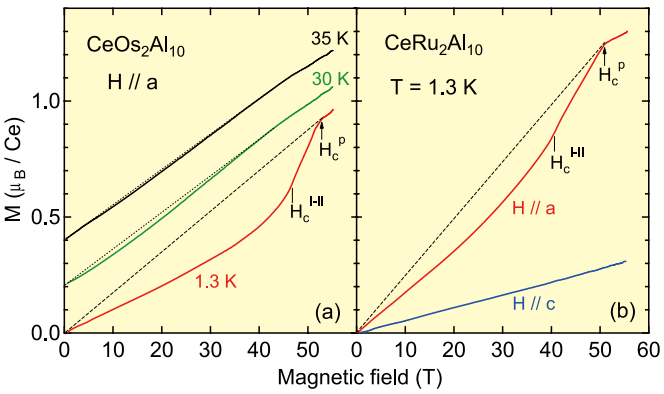

Fig. 1. (a) Magnetic field dependence of the magnetization of $CeOs_2Al_{10}$ at T = 1.3 K for H // a axis. Those at T = 30 and 35 K are also shown. The dotted lines for the results at T =30 and 35 K are drawn only to see the concave H dependence in these results. (b) Magnetization curve of $CeRu_2Al_{10}$ at T = 1.3 K for H // a axis (red upper line) and c axis (blue lower line). The dashed straight lines in (a) and (b) are drawn by connecting the origin at H = 0 and M at H_c^p.

Figures 1(a) and 1(b) represent the magnetization curves of $CeOs_2Al_{10}$ and $CeRu_2Al_{10}$ for H // a at T = 1.3 K, respectively. In Fig.1 (a), those at 30 and 35 K are also shown and in Fig.1 (b), that for H // c is shown. At T =1.3 K, magnetization (M) of $CeOs_2Al_{10}$ shows an H-linear increase up to ~ 30 T and above ~ 30 T, a concave H dependence is observed. After showing an anomaly at $H_c^{I\text{-}II}$ = 47 T, M increases steeply and shows a saturated behavior at H_c^p = 52 T. M at H_c^p is 0.95 μ_B/Ce which is smaller than 1.3 μ_B/Ce in $CeRu_2Al_{10}$, suggesting that $CeOs_2Al_{10}$ is closer to the valence fluctuation regime than $CeRu_2Al_{10}$. While both compounds show the concave M-H curve for H // a, a concave H dependence is much more pronounced in $CeOs_2Al_{10}$ than in $CeRu_2Al_{10}$. In $CeOs_2Al_{10}$, the concave H dependence is also seen at 30 and 35 K which is above T_0, although such an H dependence is not seen in $CeRu_2Al_{10}$ above T_0. This concave H dependence corresponds to the temperature of the maximum of χ_a. From these results and that of the temperature dependence of χ, we propose that a Kondo singlet accompanied by a spin gap is begins to be formed below T_{max} and coexists with the M_{AF} component parallel to c axis in the ordered state below T_0 [8].

References

[1] T. Nishioka *et al.*, J. Phys. Soc. Jpn. **78**, 123705 (2009).
[2] M. Matsumura *et al.*, J. Phys. Soc. Jpn. **78**, 123713 (2009).
[3] H. Tanida *et al.*, J. Phys. Soc. Jpn. **79**, 043708 (2010).
[4] D. D. Khalyavin *et al.*, Phys. Rev. B **82**, 100405 (2010).
[5] J. Robert *et al.*, Phys. Rev. B **82**, 100404 (2010).
[6] Y. Muro *et al.*, Phys. Rev. B **81**, 214401 (2010).
[7] D. T. Adroja *et al.*, Phys. Rev. B **82**, 104405 (2010).
[8] A. Kondo *et al.*, to be published in Phys. Rev. B.

Authors

A. Kondo, J. Wang, K. Kindo, Y. Ogane[a], Y. Kawamura[a], T. Nishioka[a], D. Tanaka[b], H. Tanida[b], and M. Sera[b]

[a]Kochi University

[b]Hiroshima University

Itinerant Electron Metamagnetic Transition in Fe_3Mo_3N

T. Waki, H. Nakamura, and K. Kindo

LiV_2O_4, Y(Sc)Mn_2 and β-Mn have attracted much attention because the Sommerfeld coefficient is enhanced in spite of the absence of localized *f*-electrons hybridizing with conduction *s*-electrons by the Kondo effect, which results in the heavy-Fermion state. The mass enhancement in these *d*-electron systems is attributed to the effect of geometric frustration inherent in their lattices, although its role in itinerant electron magnets is still under debate. As sufficient examples would give better understanding, we have focused on a new geometrically frustrated lattice, a stella quadrangula (SQ) lattice (Fig. 1(a)), and η-carbide-type compounds in which SQ sublattice is included.

Through studies of quantum magnetism of η-carbide-compounds, we found a non-Fermi liquid behavior in Fe_3Mo_3N without applying external pressure and alloying. C/T shows a divergent behavior as -log$T$ at low temperature. Together with the $T^{5/3}$ power law of resistivity, this feature suggests that Fe_3Mo_3N locates in the vicinity of a ferromagnetic quantum critical point [1]. We have confirmed that a ferromagnetic order is easily induced by the substitution of a small amount of Co [2]. On the other hand, the magnetic susceptibility shows a broad maximum at around 75 K similar to YCo_2, which undergoes a field induced transition from paramagnetic to a field-assisted ferromagnetic state called the itinerant electron metamagnetism (IEMT). Expecting a field-induced phenomenon, we performed high field magnetization measurements on Fe_3Mo_3N.

Figure 1 (b) illustrates the magnetization of Fe_3Mo_3N measured at several temperatures. At the lowest temperature, it shows a discontinuous jump at around 13.9 T with small hysteresis ΔH revealing that the transition is of first order. Typical IEMT materials show rapid but not sharp increase

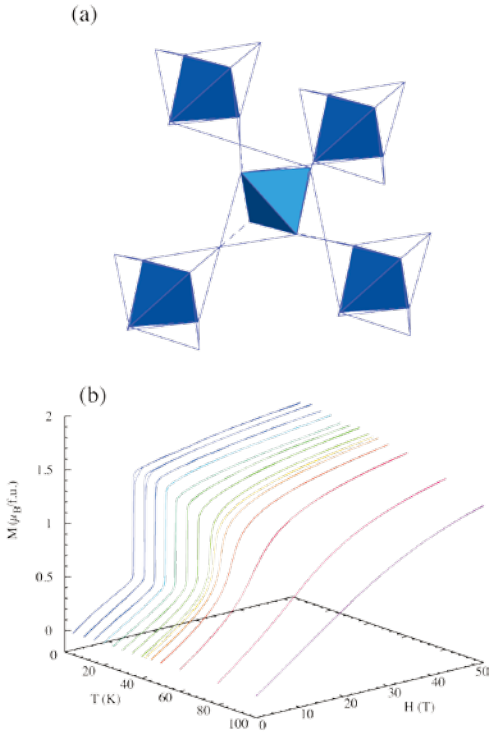

Fig. 1. (a) A sketch of the stella quadrangula lattice. (b) High field magnetization measured at several temperatures. At the lowest temperature, a quite sharp metamagnetic transition was observed at 13.9 T.

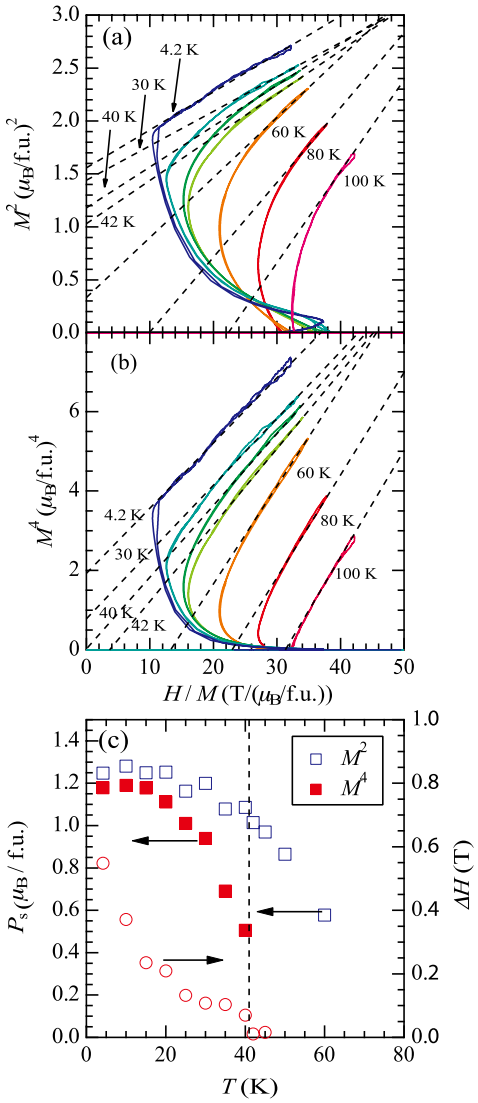

Fig. 2. (a) M^2 vs H/M plot. (b) M^4 vs H/M plot. (c) Temperature dependences of hypothetical spontaneous moment P_S and ΔH.

and relatively large hysteresis. With increasing temperature, the transition field increases following a T^2 power relation $H_C(T)$ = 13.84 + 0.00107 T^2 in agreement with the other IEMT materials. The critical temperature is determined as the point where the hysteresis disappears. The first order transition terminates at (42 K, 15.8 T). Since Fe_3Mo_3N is in a field induced ferromagnetic state at the high magnetic field region, good linearity of the Arrott plot (M^2 vs H/M) is expected. It is linear at the lowest temperature, but poorly linear at high temperatures (Fig. 2(a)). On the other hand, interestingly, M^4 vs H/M plots give good linearity in a wide temperature range (Fig. 2(b)). Furthermore, the hypothetical spontaneous moment estimated from the intersection of the M^4 vs H/M relations disappears at around 40 K in agreement with T_C determined from the hysteresis.

The disappearance of the fourth order expansion coefficient of free energy at T_C, resulting in the linear relation of M^4 vs. H/M, has been proposed by Takahashi to explain the magnetization of MnSi based on the spin fluctuation theory including the effect of zero point fluctuations [3]. The liner relation of M^4 vs H/M is, in general, valid for the magnetization at around T_C. As the critical region is often expanded by a low dimensional dispersion, our result possibly suggests that the critical region is expanded by the reduction of correlation length associated with the geometric frustration in the stella quadrangula lattice.

References
[1] T. Waki, *et al*., J. Phys. Soc. Jpn. **79**, 043701 (2010).
[2] T. Waki, *et al.*, EPL **94**, 37004 (2011).
[3] Y. Takahashi, J. Phys. Soc. Jpn. **55**, 3553 (1986); Y. Takahashi, J. Phys.: Condens. Matter **13**, 6323 (2001) and references therein.

Authors
T. Waki[a], S. Terazawa[a], Y. Tabata[a], H. Nakamura[a], A. Kondo, K. Sato, and K. Kindo
[a]Kyoto University

International Conferences and Workshops

The Horiba-19th International Conference on the Application of High Magnetic Fields in Semiconductor Physics and Nanotechnology (HMF-19)

August 1-6, 2010
Fukuoka International Congress Center
S. Takeyama (Chair)

The HMF-19 has been held at Fukuoka International Congress Centre, facing the Hakata bay, as a satellite conference of the International Conference on the Physics of Semiconductors (ICPS-2010, Seoul, Korea, July 25-30). The HMF-19 follows up outstanding meetings organized by predecessors in São Pedro (2008), Würzburg (2006), and so on, since 1972. The HMF-19 will become the 4th one held at Japan after Hakone, Tomiura, and Matsue. The program was arranged so that stimulating discussions were possible among participants by allotting sufficient discussion time and by avoiding parallel sessions. The scope of this conference covered all the new topics of basic and applied semiconductor related physics coming to light in magnetic fields as follows in High Magnetic Fields; Integer and Fractional Quantum Hall Effects, Quantum Dots, Graphene, Carbon Nanotubes, Magneto-Optics, Magneto-Tunneling and General Magneto-Transport, Magnetic Resonance (ESR, NMR), Novel Experimental Techniques in High Magnetic Fields, Electron Correlation and Emergent Phases in High Magnetic Fields, Spin-Related Phenomena, Organic Conductors, and Nanowires. 168 participants including 27 oversea and 10 domestic invited speakers have been rapt in hot discussion on the subjects of current topics. There were many interesting presentations of the hot subject of 'Graphene'. More than half of the participants were from 20 different oversea countries. The afternoon poster session was placed at the main big hall in front of the lecture room, and hot discussion was held in front of more than 80 posters with beer and plenty of good foods.

This conference was financially supported by Tokyo University Horiba Kokusai Fund (donated by Dr. Masao Horiba, the founder of Horiba Ltd.), Fukuoka city, the ISSP, the Univ. of Tokyo, and the Global Center of Excellence for Physical Science Frontiers, Univ. of Tokyo. Program chair was undertaken by Dr. K. Muraki (NTT Basic Research Lab), the conference secretary by Prof. T. Machida (IIS the Univ. of Tokyo), local organizing chair by Prof. K. Oto (Chiba univ.), and an accountant by Prof. Y. H. Matsuda (ISSP).

The ISSP International Workshop on Soft Matter Physics

August 9-13, 23-27, 2010

H. Noguchi, S. Fujii, S. Komura, H. Orihara, T. Taniguchi, M. Imai, T. Toyota, M. Shibayama, H. Endo, and H. Shiba

The ISSP International Workshop on Soft Matter Physics" (ISSP/SOFT2010) was held for two weeks, for August 9-13, 2010 and August 23-27. The topic of the first week (Aug. 9-13) was Structural Rheology, the relation between reology and mesoscale structure in soft matter. In the second week (Aug. 23-27), we focused on Biomembranes and Vesicles. We arranged this workshop to connect two other conferences seamlessly to form "Soft-Matter Month in Japan" in August 2010. Between two sessions of our workshop, a symposium on soft matter was held in Nara on 17-20 Aug. 2010: International Symposium on Non-Equilibrium Soft Matter 2010. In the previous week (Aug. 1-6) of our workshop, 5th Pacific Rim Conference on Rheology was held in Sapporo. We had 57 and 80 participants for the first and second weeks, respectively. Despite of hot weather, very active discussions were done for oral and poster presentations.

For the most of the period (Aug. 9-13 and Aug. 25-27), the workshop was held at ISSP. On Aug. 23, the Special Intensive Lectures were held at Ochanomizu University and on Aug. 24, the workshop was held at Institute for the Physics and Mathematics of the Universe (IPMU). The workshop was supported by ISSP and Institute for Complex Adaptive Matter (ICAM-I2CAM).

The program and other details of the Workshop can be found at the Workshop web page: http://www.issp.u-tokyo.ac.jp/public/soft2010/

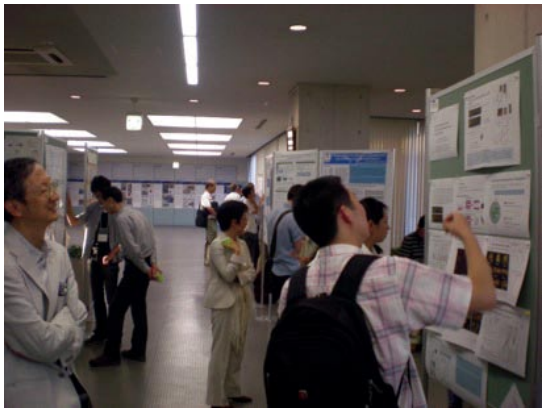

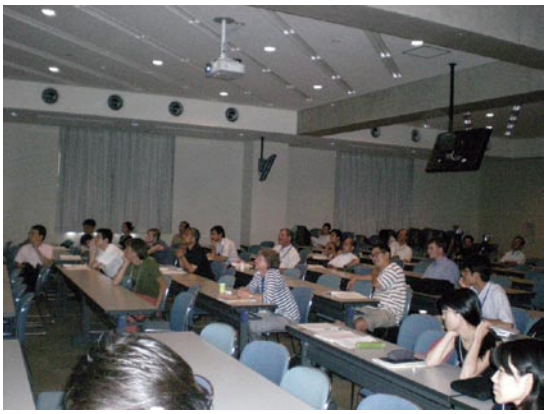

Spin-related Phenomena in Organic Materials

July 1-3, 2010

H. Tajima, K. Kanoda, M. Yamashita, S. Uji, T. Mori, H. Mori, M. Takigawa, T. Osada, T. Kato, and M. Shiraishi

Understanding of electrical conduction in organic materials has increased over the past 50 years. From the viewpoint of basic science, the focus has been on the study of single crystals of various organic materials, and CDW, SDW, and superconductive states have been found. From the viewpoint of applied science, the focus has been on the design of electronic devices of organic materials, and various organic devices, such as OLEDs and OFETs, have been prepared. Although, the initial strong interaction between researchers in basic and applied sciences decreased, there has been a renewed interest in working together to expand this field.

The interplay between π conduction electrons and spin degrees of freedom is of current interest in organic solid state physics. Researchers have investigated this interplay from the viewpoints of both basic science and device physics. This workshop was organized to bring those researchers together to discuss various aspects of the "spin-related phenomena" with the hope of further developing this field. Topics discussed in the workshop included: i) organic spintronics, ii) *d*-π molecular conductors and giant negative magnetoresistance, iii) molecular magnets, and iv) charge order and related phenomena in molecular conductors. With 32 talks, 25 posters, and approximately 90 participants, including 14 from abroad, the discussion at the workshop was very active and fruitful, indicating strong interests in the field. The program and other details of the workshop can be found at the workshop web page (http://tajima.issp.u-tokyo.ac.jp/ workshop20100701/index.htm).

This international workshop was planned as a part of the International Conference on Science and Technology of Synthetic Metals 2010 (July 4-9, Kyoto) and was sponsored by ISSP, a Grant-in-Aid for Scientific Research on Innovative Areas (New Frontier of Materials Science Opened by Molecular Degrees of Freedom: MDF), and the Yamashita Project of Tohoku University.

ISSP Workshops

Metal-Insulator Transitions in Pyrochlore Oxides

May 26-27, 2010
Z. Hiroi

Recently, great attention is focused on the physics of the frustrated lattice. The most studied are transition metal oxides, such as pyrochlore and spinel oxides comprising pyrochlore lattices. It has been recognized that, in these materials, interplay between charge, spin and orbital degrees of freedom gives rise to many interesting physical properties including a metal-insulator transition.

In this workshop, metal-insulator transitions in some transition metal pyrochlore oxides were focused, and various experimental and theoretical contributions were exchanged among participates with the aim to reveal their features. In particular, $Cd_2Os_2O_7$, which shows a metal-insulator transition at rather high temperature of 230 K accompanied by a magnetic order without any symmetry change in the crystal structure, has been discussed.

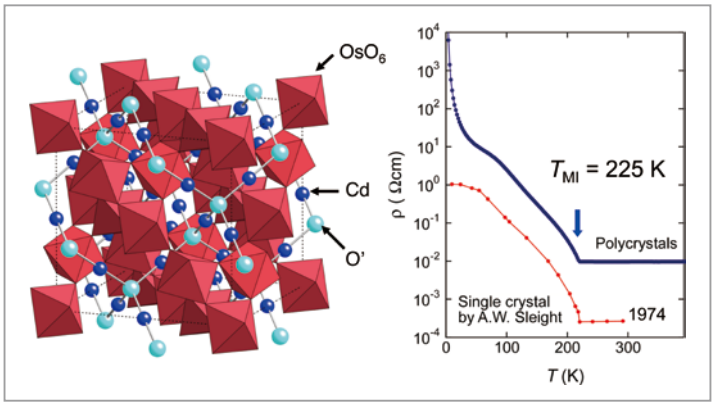

Time Domain Control of External Field and Real-Time Physical Phenomena

June 22-23, 2010
H. Nojiri, S. Takeyama, T. Suemoto, M. Oshikawa, S. Miyashita, and H. Ohta

Various phase transitions in equilibrium, induced by a change in parameters such as magnetic field, pressure, and temperature, have been studied. Recently, however, there is a growing need of understanding physical phenomena, explicitly including time dependence. Examples include coherent spin manipulation, exciton dynamics, photo-induced phase transition, Bose-Einstein condensation, high-spin/low-spin transition, kinetics of first-order transitions, magnetic resonance, and magnetic relaxors. These days, these systems can be controlled through external fields such as electromagnetic field, with high precision, high speed, and detailed programmability. This has been made possible by the rapid development in coherent light sources and progress in understanding of quantum dynamics with magnetic field as the control parameter, to name but a few. This workshop was organized in order to gain unified understanding, from the view point of real-time dynamics, of a wide variety of responses and phase transitions that are induced by time domain control of external field. Reflecting this concept, 28 talks and 14 posters on very diverse topics, ranging from graphite-diamond transition to quantum measurement problem, both experimental and theoretical, were presented. Special care was taken to encourage questions and discussions across different disciplines.

Recent Problems in Physics of Glasses --- Interface between Experiments and Theories

November 29 - December 1, 2010
T. Odagaki, R. Nozaki, J. Habasaki, K. Fukao, and O. Yamamuro

The research of glasses and glass transitions may be the last frontier of condensed matter physics left for this century. In the last decade, Japanese scientists have accomplished many important works in this field. Since 2002, we have held the meetings on glasses every two years as ISSP workshops. This is the forth meeting. In the present workshop, we had 33 oral and 20 poster presentations and the number of total participants was 80. Theoretical, computer simulation and experimental researchers presented their recent works on the glass transitions and related phenomena. In the theoretical sessions, the works on current important models, *e.g.*, the mode-coupling, replica, and free-energy landscape theories, were presented. There was exciting discussion on the relation between the above models, and also on the relation between the dynamical heterogeneity and static structures in supercooled liquids. There were various computer simulation studies not only for conventional simple systems to test the theoretical predictions but also for the realistic glass-formers, e.g., ionic liquids, silicates, etc. Various experimental results were shown for the glasses of vapor-deposited molecules, polymers, polymer thin films, etc. There were also interesting talks on water and aqueous solutions, especially on water confined in nano-porous materials. Throughout the workshop, we had fruitful discussion to clarify the interface between the experiments and theories including computer simulations and also to reorganize the remaining problems in physics of glasses.

Challenge and Perspective of Computational Materials Science

January 5-7, 2011
H. Noguchi, N. Kawashima, O. Sugino, S. Tsuneyuki, T. Suzuki, Y. Tomita, Y. Noguchi, H. Shiba, and H. Watanabe

Every year, we hold a workshop for the joint research of the ISSP supercomputers. This year, we combined it with two workshops. 1) The first annual workshop of Computational Materials Science Initiative (CMSI), which started on September 2010 for Next-Generation Supercomputer Strategy Program Field 2 ”New Materials and Energy Creation”. 2) The annual workshop of the next-generation functional nanomaterials for information technology in the next-generation supercomputer project, Grand Challenges in Next-Generation Integrated Nanoscience.

During the three days, we had 36 oral presentations, 72 poster presentations and a lot of active discussions that follow the presentations. More than 100 scientists participated every day not only from solid state physics, but also from molecular science and materials science. The subjects of the presentations ranged from the most fundamental low-temperature behaviors of quantum matters to semi-conductor devise, functional designs of large molecules and new energy resources. We also evaluated talks from the viewpoint of massive parallelism on new architectures. Based on the results of the reviews by the executive committee of CMSI, three young researchers were awarded with CMSI poster prizes: Takahiro Misawa (Best Poster prize, Univ. Tokyo), Hidemaro Suwa (Excellent Poster prize, Univ. Tokyo) and Hayato Shiba (Reviewers Special prize, ISSP).

ISSP Workshop on "Developments and Science by Neutron Scattering Spectrometers" —Small-angle, Reflectivity, and High-resolution Spectrometers—

February 7-8, 2011
M. Hino, H. Endo, O. Yamamuro, and M. Shibayama

Instrumentation and Research Teams (IRTs) of the neutron scattering spectrometers installed at JRR-3 research reactor (Tokai, Japan) have been promoting the General User Program (GUP) of neutron scattering as well as their own research projects. A workshop organized by IRTs was held at ISSP, Kashiwa, to discuss various aspects of neutron science and instrumentation. Topics discussed in this workshop included small-angle neutron scattering (SANS-U), neutron spin echo (iNSE) and angle focusing cold neutron (AGNES) spectrometers and multilayer interferometer and reflectmeter for neutron (MINE-1 and 2). Up-dated specification and performance of these instruments together with recent experimental results obtained by general users were presented by 28 speakers, and future directions of GUP were extensively discussed.

Tsukuba Soft Matter Workshop 2011

March 7-8, 2011
M. Shibayama, H. Noguchi, K. Fujii, H. Shiba, and H. Seto

The 3rd Tsukuba Soft Matter Workshop was held in Kashiwa Campus, the University of Tokyo, during the period of Mar. 7-8, 2011. Tsukuba area, which is very close to Kashiwa Campus of the University of Tokyo, has been one of the active centers on soft matter physics and chemistry in Japan. In the beginning, the workshop was mainly devoted to exchange ideas and information on structure and dynamics of complex fluids, such as, liquid crystals, surfactants, and gels. Recently, several groups on theory and simulation have launched their activities. In this workshop, a (not too large) workshop has been held for two days to exchange information on their recent activities. In spite of snowy and cold days, we had about 50 attendants in total, not only from Tsukuba area but also from Hongo campus, Kyoto University, and so on. Very intensive discussions have been held on the presentations mainly about gels and molecular simulations.

A proceeding booklet which contains the presentation slides (mainly in Japanese) is available (contact: Prof. Shibayama, Neutron Science Lab).

New Opportunities in Solid State Physics at High Brilliance Soft X-ray Beamline, SPring-8 BL07LSU of the University of Tokyo

March 8, 2011
S. Shin, I. Matsuda, and A. Kakizaki

The construction of the new undulator beamline at the SPring-8, BL07LSU, was finished two years ago and since then, the high brilliance synchrotron light within the energy range from 250 eV and 2 keV is applied for the advanced solid state spectroscopy. The aim of the workshop is to discuss the recent results obtained at this beamline under the research proposals by construction teams and general users. After a brief report on the present status of the polarization controlled undulator and the characteristics of the beamline, the new scientific achievements of three main topics of the research program were presented. It was reported that main apparatuses, three-dimensional (3D) nano-ESCA, soft X-ray emission spectroscopy (XES) and time-resolved photoemission apparatuses, achieved high performances as they initially expected: (3D) nano-ESCA shows the spatial resolution below 70 nm, XES spectra with energy resolution lager than 10,000 was obtained and time- and momentum-resolved photoemission spectra were measured synchronized with femto-second laser pulses. The results of soft X-ray diffraction experiments to investigate characteristics of hidden surfaces and interfaces and photoelectron diffraction experiments were also presented in the workshop. In the workshop, more than 40 participants including many young scientists also discussed on the new scientific opportunities and future research works not only at BL07LSU, but other undulator beamines at SR facilities such as UVSOR, KEK-PF and HiSOR.